Optimization of evaporative cooling of Rubidium atoms in a magnetic trap

Pieter Valkering

February 1999

Thesis for graduation in experimental physics

at the University of Utrecht

Supervisors:

Kai Dieckmann

Jook Walraven

Working group of: Prof. Dr. J.T.M. Walraven

FOM Institute for Atomic and Molecular physics, AMOLF

Amsterdam

Contents

Chapter 1

Introduction and outline

1.1 Bose Einstein Condensation

The phenomenon Bose Einstein Condensation (BEC) was predicted in the early days of quantum mechanics by Bose and Einstein [1]. For a system of weakly interacting Bosons confined in a box, it was found that at a small, but finite temperature a large fraction of the Bosons would go into the lowest energy level, thus forming a Bose-Einstein condensate. The major physical significance of BEC is that the condensate is a system, which shows quantum mechanical behavior on a mesoscopic scale. As such, BEC is related to phenomena like superfluidity and superconductivity.

The condition for BEC to occur is that the thermal de Broglie wavelength $\Lambda = \sqrt{2\pi\hbar^2/(mkT)}$ is of the order of the interatomic spacing. For atomic gasses this can only occur for extremely low temperatures. For example, for alkali-vapors at a density around 10^{14} particles per cubic centimeter the critical temperature is of the order 1 μK. Over the last twenty years, several techniques were developed to cool atomic gasses, nearly reaching the transition point. The key to BEC was found in a combination of two different technologies: laser cooling and magneto-optical trapping, and evaporative cooling and magnetic trapping. This resulted in the year 1995 in the experimental observation of BEC with the alkali elements Rubidium, Sodium and Lithium ([2], [3], [4]).

1.2 Evaporative cooling in the experiment

The goal of the experiment performed at AMOLF is to obtain BEC with ^{87}Rb atoms. This will provide an environment for further study of the properties of the condensate. Very briefly, the experiment can be described as follows. Laser cooling and magneto-optical trapping techniques are applied to obtain a precooled atomic gas sample of $\sim 10^9$ atoms in an ultra high vacuum glass cell. The laser light is then switched off and the sample is transferred to a magnetic trap. After an adiabatic compression stage, the density of the atomic

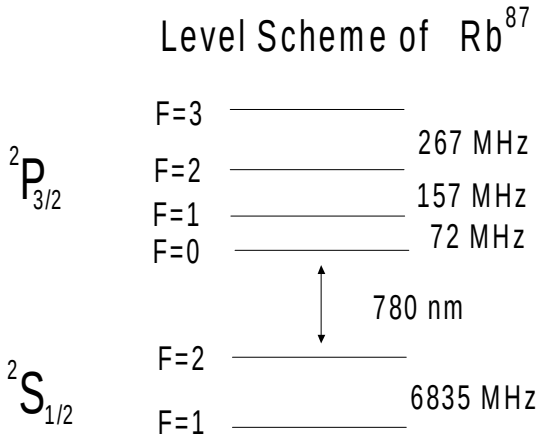

Figure 1.1: The level scheme of ^{87}Rb. The magnetically trapped atoms are prepared to be in the $^2\mathrm{S}_{1/2}$, $F = 2$, $m_F = 2$ state.

sample $n \sim 10^{12}$ cm^{-3} and the temperature $T \sim 300$ μK, corresponding to a phase-space density $n\Lambda^3$ of the order 10^{-6}. Finally, the sample is cooled to the BEC transition by evaporative cooling. At the current stage in the experiment, atoms can be loaded into a magneto optical trap (MOT) and the transfer to the magnetic trap will be soon established. The initial values for evaporative cooling of density and temperature given here are based on previously performed experiments in other groups under similar conditions, see for example **??**.

In this report we will focus on the final stage of the cooling process: evaporative cooling in a magnetic trap. The principle of magnetic trapping is based on the following. A particle with a magnetic moment $\vec{\mu}$ placed in a magnetic field $\vec{B}$ experiences a potential $U(\vec{x}) = -\vec{\mu} \cdot \vec{B}$. When $\vec{\mu}$ is directed parallel to the magnetic field the particle moves under influence of the magnetic force $\vec{F} = -\vec{\nabla}U$ towards a region of high magnetic field. These particles are called "high field seekers". On the contrary, when $\vec{\mu}$ is directed anti-parallel to the magnetic field it tends to move towards a region of low magnetic field. These particles are referred to as "low field seekers". Since only local minima in the magnitude of a B-field can exist in a current free region [6], only low field seekers can be trapped. Therefore, magnetically trapped atomic clouds are prepared in such a way as to have all their spins pointing parallel to the magnetic field. This is called "spin polarization". In our experiment, the ^{87}Rb atoms are optically pumped to the $^2S_{1/2}$, $F = 2$, $m_F = 2$ state during the transfer from the MOT to the magnetic trap (see figure 1.1). The spin states $m_F = 2$ and $m_F = 1$ are referred to as "trapped" states and the other three m_F states are referred to as "untrapped" states.

Atoms in magnetic traps are cooled by evaporative cooling, which is described in Chapter 4. The process is based on the selective removal of particles with energies higher than the mean energy per particle and on thermalization by elastic collisions. This is similar to for example the cooling of hot water due to evaporation of water molecules. It is a very powerful technique that can increase phase space density over many orders of magnitude with relatively low particle loss. Selective removal of atoms can be accomplished by selectively inducing transitions to untrapped states, where for the shallow magnetic trapping potentials used, the Zeeman splitting corresponds to frequencies in the radio frequency regime. This process is described in Chapter 3. When the transition is sufficiently saturated, all atoms with an energy higher than a certain threshold value, the so called truncation energy ε_t, can be continuously removed from the trap. The system effectively cools when the truncation energy is chosen to be in the order of several times the mean energy per remaining atom $\sim kT$. As the temperature of the atomic gas drops about two orders of magnitude during the cooling process, the truncation energy has to be lowered accordingly.

The first goal of my work was to calculate of the efficiency of the rf-transition for realistic parameters during evaporative cooling. On the basis of the results the intensity of the rf-field needed for efficient evaporative cooling was fixed. Also technical aspects of the implementation of the rf-circuit were considered. The main goal of my work was to optimize the evaporation ramp, i.e. to determine how to install and lower the evaporation barrier in such a way as to reach the on-set of BEC with minimal particle loss. This optimization was done by numerical simulation of the cooling process based on an analytical model describing the thermodynamics of the atomic cloud. As a whole, this thesis forms a fairly complete study of evaporative cooling for Rubidium atoms in a magnetic trap.

Chapter 2

The magnetic trap

2.1 Trap design

Many different magnetic trap configurations have been used to trap atomic gas samples. In our experiment we use so called the Ioffe trap. It consists of two "axial coils", two "compensation coils" and four straight bars called "Ioffe bars", with currents flowing as indicated in figure 2.1. The coils are wound from square copper wire, which is hollow to allow water cooling. The currents are provided by a HP model 6681A power supply, that is able to provide currents up to 580 A.

The field components of the Ioffe trap near the trap center, described in cylindrical components, are found from [7] and are given by

$$\begin{aligned} B_z &= B_0 + bz^2, \\ B_\rho &= -a\rho \sin 2\phi - b\rho z, \\ B_\phi &= -a\rho \cos 2\phi, \end{aligned} \tag{2.1}$$

where z denotes the axis of axial symmetry. The field gradient in the lateral direction a is provided by the Ioffe bars and the axial curvature b is primarily provided by the axial coils. The off-set field generated by the axial coils is compensated by the compensation coils to yield a small value B_0, thereby slightly reducing the axial curvature. Using a by-pass over the compensation coils the value of B_0 can be tuned.

The parameters a and b from (2.1) were determined from magnetic field measurements at low currents ($I = 40$ A). The field was measured using a F.W.Bell Gaus meter with a resolution of 0.1 G. The meter essentially consists of a Hall probe with an active area of 0.18 mm in diameter. Using an assembly of translation stages the probe could be moved through the interior of the magnetic trap independently in three dimensions.

Figure 2.2 shows the magnetic field component along the vertical direction at $z = 0$ as produced by the Ioffe bars. The data points are well fitted and yield a gradient $a' = 0.353$ T/m. In figure 2.3 the axial field component along

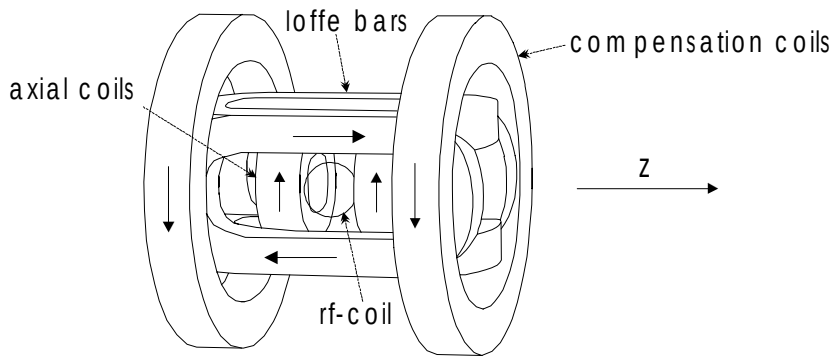

Figure 2.1: The Ioffe trap: Shown are the "axial coils", the "compensation coils" and the "Ioffe bars", where currents are flowing as indicated by the arrows. The rf-coil is positioned in between the axial coils. The z-axis is taken to be the axis of axial symetry.

the z-axis as produced by the axial coils together with the compensation coils is shown. Again the data points are well fitted, yielding a gradient $b' = 14.0$ T/m^2. For a realistic current of 400 A. during the experiment, we obtain the values $a = 3.53$ T/m and $b = 140$ T/m^2.

2.2 The rf-coil

The position of the rf-coil in the magnetic trap is shown in figure 2.1. The rf-coil is fitted in between the axial coils, which yields a maximum outer diameter $d = 31$ mm. For a coil of two windings and wirethickness ~ 1mm, the distance between the center of the coil and the center of the magnetic trap must be at least 17 mm.

The magnetic field geometry in relation to the direction of the rf-field is shown in figure **??**. Well away from the center of the magnetic trap the magnetic field is dominated by the quadrupolar field of the Ioffe bars. For this case the rf-field is directed parallel to the magnetic field lines in the x-direction and directed perpendicular to the magnetic field lines in the y-direction. Near the center of the magnetic trap the magnetic field is dominated by its component B_0 in the axial direction z (shown in the picture as an arrow tail in the center), so that the rf-field is always directed perpendicular to the trapping field.

2.3 Trapping potential and density of states

The magnitude of the magnetic field $|\vec{B}|$ near the field center is obtained from equation (2.1). Neglecting all terms of order higher than ρ^2 and using $bB_0 \ll a^2$

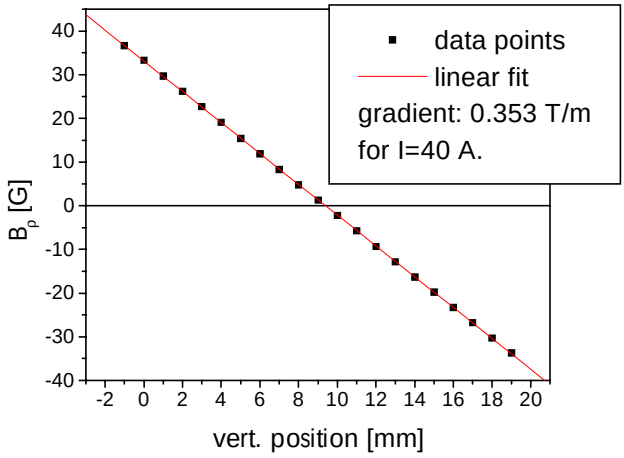

Figure 2.2: Measurement of the magnetic field component along the vertical direction at $z = 0$ as produced by the Ioffe bars for a current $I = 40$ A. For a realistic current $I = 400$ A during the experiment, we obtain for the field gradient $a = 3.53$ T/m.

one finds

$$|\vec{B}| = \sqrt{a^2\rho^2 + (B_0 + bz^2)^2}. \tag{2.2}$$

The associated magnetic trapping potential is given by

$$V_B(\rho, z) = g_F \mu_B m_F \left(|\vec{B}| - B_0\right) = \sqrt{\alpha^2\rho^2 + (U_0 + \beta z^2)^2} - U_0, \tag{2.3}$$

which is set to zero in the trap center. The radial gradient α, the axial curvature β and the parameter U_0 are defined as $\alpha \equiv g_F \mu_B m_F a$, $\beta \equiv g_F \mu_B m_F b$ and $U_0 \equiv g_F \mu_B m_F B_0$.

All relevant information about the trapping potential is contained in the density of states, given by

$$\rho(\varepsilon) = \int d\mathbf{r}d\mathbf{p}\ \delta[\varepsilon - U(\mathbf{r}) - p^2/2m]. \tag{2.4}$$

Evaluating the momentum integral one finds

$$\rho(\varepsilon) = \frac{2\pi(2m)^{3/2}}{(2\pi\hbar)^3} \int_{U(\mathbf{r})\leq\varepsilon} d\mathbf{r}\sqrt{\varepsilon - U(\mathbf{r})}. \tag{2.5}$$

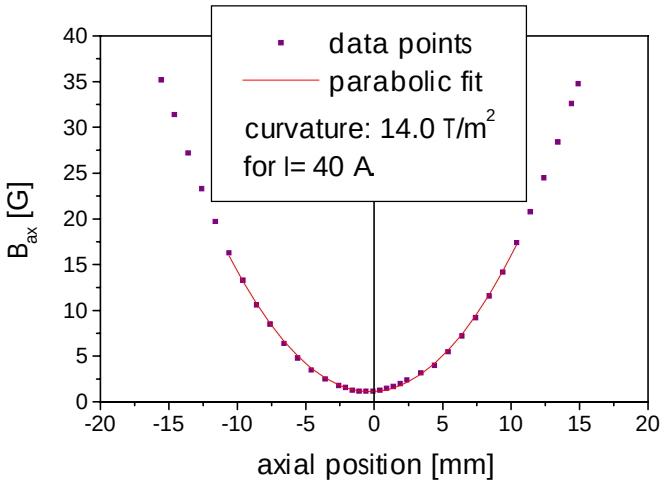

Figure 2.3: Measurement of the axial field component along the z-axis as produced by the axial coils together with the compensation coils for a current $I = 40$ A. For a realistic current $I = 400$ A during the experiment we obtain for the axial curvature $b = 140$ T/m^2.

For a whole class of potentials, the so called power-law traps, equation 2.5 yields

$$\rho(\varepsilon) = A_{PL}\varepsilon^{1/2+\delta}, \tag{2.6}$$

where A_{PL} is a trap dependent constant. These include square ($\delta = 0$), harmonic ($\delta = 3/2$) and spherically symmetric traps, with $U(r) \sim r^{3/\delta}$, as well as potentials of the form $U(x, y, z) \sim |x|^{1/\delta_1} + |y|^{1/\delta_2} + |z|^{1/\delta_3}$, with $\delta = \sum_i \delta_i$. The density of states in the Ioffe trap is found by substituting the Ioffe trapping potential (2.3) into (2.5). This yields a sum of quadratic ($\delta = 3/2$) and cubic ($\delta = 5/2$) terms

$$\rho(\varepsilon) = A_{IQ(}\varepsilon^3 + 2U_0\varepsilon^2), \tag{2.7}$$

where $A_{IQ} = (2m\pi^2)^{3/2}/[(2\pi\hbar)^3 2\alpha^2\beta^{1/2}]$. It is readily seen that for temperatures $kT \gg U_0$ the density of states (2.7) will effectively be the one of a power-law potential $\delta = 5/2$. This corresponds to the case $\alpha^2\rho^2 \gg U_0$ in trapping potential (2.3), so that the potential is effectively linear in the radial direction. For temperatures $kT \ll U_0$ the density of states is effectively harmonic ($\delta = 3/2$). This corresponds to the case $\alpha^2\rho^2 \ll U_0$ in the trapping potential (2.3), so that the potential is effectively linear in the radial direction.

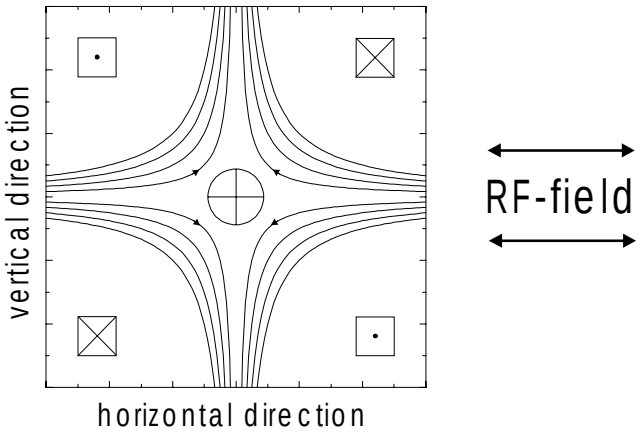

Figure 2.4: The magnetic field geometry in relation to the direction of the rf-field. This picture represents a crossection through the trap center ($z = 0$) perpendicular to the Ioffe bars. Well away from the center of the magnetic trap the magnetic field is dominated by the quadrupolar field of the Ioffe bars. For this case the rf-field is directed parallel to the magnetic field lines in the x-direction and directed perpendicular to the magnetic field lines in the y-direction. Near the center of the magnetic trap the magnetic field is dominated by its component B_0 in the axial direction z (shown in the picture as an arrow tail in the center), so that the rf-field is always directed perpendicular to the trapping field.

Chapter 3

Inducing hyperfine transitions with RF

3.1 Introduction

Magneticaly trapped atoms can be removed from the trap by inducing transitions to untrapped hyperfine spin states. This is done by applying an oscillating magnetic field with a linear polarization transverse to the static trapping field $\vec{B}$. The surface in space where transitions may occur, is determined by the resonance condition

$$g_F \mu_B |\vec{B}(\vec{x}_{\rm res})| = \hbar\omega_{\rm rf}, \tag{3.1}$$

with $\omega_{\rm rf}$ the frequency of the oscillating magnetic field, g_F the Landé g-factor and μ_B the Bohr magneton. For typical trapping fields of 10^{-3} T, $\omega_{\rm rf}$ is in the radio-frequency regime.

When $\omega_{\rm rf}$ is chosen so that resonance occurs at the edges of the trap, the atoms of low energy, that remain mostly near the center of the trap, are unaffected. However, the atoms that have enough energy to reach the edges of the trap will pass through a region of resonance and transitions to untrapped states will occur. If this transition is sufficiently saturated, effectively all atoms with an energy higher than a certain threshold value will evaporate from the trap.

The main part of this chapter is devoted to a calculation of the transition probability to untrapped spin states for our 5-level Rubidium atom for realistic experimental conditions. This will be done on the basis of the "dressed state" formalism [8] and involves numerical solution of the time dependent Schrödinger equation. On the basis of these results, the rf-field amplitude that will provide efficient evaporative cooling is determined. Finally, technical aspects of the implementation of the rf-circuit will be considered.

3.2 Interaction with a rf-field

3.2.1 The Hamiltonian

Assuming that the atom is following a classical trajectory, the situation of an atom moving in a magnetic field with a field gradient is equivalent to the situation of an atom at rest in a time varying magnetic field. The latter point of view will be adopted here.

The Hamiltonian for a spin in a time varying magnetic field $\vec{B}(t)$ is given by

$$H(t) = \gamma \vec{B}(t) \cdot \vec{F}, \tag{3.2}$$

with $\vec{F}$ the operator of total angular momentum and $\gamma \equiv \frac{g_F \mu_B}{\hbar}$ a constant. The magnetic field consists of a contribution of the trapping field B_{trap} directed along the z-axis and a contribution from the rf-field. Assuming a linearly polarized rf-field with the magnetic field component directed along the x-axis perpendicular to the trapping field, the magnetic field is expressed as

$$\vec{B}(t) = B_{\mathrm{trap}} \hat{z} + B_{\mathrm{rf}} \cos(\omega_{\mathrm{rf}} t) \hat{x}, \tag{3.3}$$

with B_{rf} the amplitude of the rf-field and ω_{rf} its frequency. Substituting this expression for the magnetic field into the Hamiltonian (3.2) yields

$$H(t) = \omega_0(t) F_z + 2\omega_R \cos(\omega_{\mathrm{rf}} t) F_x, \tag{3.4}$$

with $\omega_0(t) = \gamma B_{\mathrm{trap}}(t)$ the time dependent Zeeman shift and $\omega_R = \frac{1}{2}\gamma B_{\mathrm{rf}}$ a measure of the intensity of the rf-field analogous to the Rabi frequency for a two level system. Energy and spin are measured in units of $\hbar$.

3.2.2 Rotating frame and rotating wave approximation

This system is most easily treated in a rotating coordinate system, turning around the z-axis with frequency ω_{rf} [8]. The operator U generating this rotation is given by:

$$U(t) = e^{-i\omega_{\mathrm{rf}} t F_z}. \tag{3.5}$$

Instead of the usual basis of m_F states $|\alpha_m>$ we use rotating basis vectors given by

$$|\alpha_m^r(t)> = U(t)|\alpha_m> \tag{3.6}$$

and the state vectors $|\Psi(t)>$ transform as

$$|\Psi^r(t)> = U^{-1}(t)|\Psi(t)>, \tag{3.7}$$

where the subscript r denotes the rotating co-ordinate frame. The Hamiltonian in the rotating frame must be the operator generating the time evolution:

$$i\frac{\partial}{\partial t}|\Psi^r(t)>= H^r(t)|\Psi^r(t)> . \tag{3.8}$$

Substituting (3.7) into (3.8) and using $i\frac{\partial\Psi}{\partial t} = H\Psi$, we find that the Hamiltonian in the rotating frame must be given by

$$H^r(t) = U^{-1}H(t)U + i\dot{U}^{-1}U, \tag{3.9}$$

where the explicit time dependence of U has been omitted for convenience.

Let's look somewhat closer at the obtained result. The first part to the right of equation (3.9) is given by:

$$U^{-1}H(t)U = \omega_0 F_z + \omega_R F_x + \omega_R F_x \cos 2\omega_{\mathrm{rf}} t + \omega_R F_y \sin 2\omega_{\mathrm{rf}} t. \tag{3.10}$$

The last three terms on the right of (3.10) have a straight forward physical interpretation. The linearly polarized rf-field can be regarded as the sum of two counter-rotating circularly polarized fields. In the rotating frame the co-rotating component appears static, while the counter-rotating component rotates at twice the frequency. Perturbation theory shows that this quickly oscillating term can be neglected. This is known as the rotating wave approximation.

Apart from the ordinary transformation Hamiltonian $U^{-1}H(t)U$, an extra term has been added to H_r, which must be taken into account for any time dependent transformation. In our case it is given by:

$$i\dot{U}^{-1}U = -\omega_{\mathrm{rf}} F_z. \tag{3.11}$$

Thus, the interaction energy with the magnetic field has been decreased by a number of m_F photon energies. The approximated Hamiltonian in the rotating coordinate system can now be written as

$$H^r(t) = \Delta(t)F_z + \omega_R F_x, \tag{3.12}$$

where the detuning Δ is introduced as

$$\Delta(t) \equiv \omega_0(t) - \omega_{\mathrm{rf}}. \tag{3.13}$$

The thus obtained approximated Hamiltonian is of a very simple form and is only implicitly time dependent by the time dependence of $\Delta(t)$. For a five-level spin system (F=2) the energy eigenvalues are calculated and plotted as a function of Δ in figure 3.1. Far off resonance, the eigenstates of H^r coincide with the eigenstates of the non-interacting system. For each eigenvalue a number of photon energies have been added as to make them cross at resonance $\Delta = 0$. The presence of the perturbation term turns this crossing into an avoided crossing. Here, an eigenstate of H^r will be a superposition of the eigenstates of the unperturbed system. This means that near resonance, one can not speak of

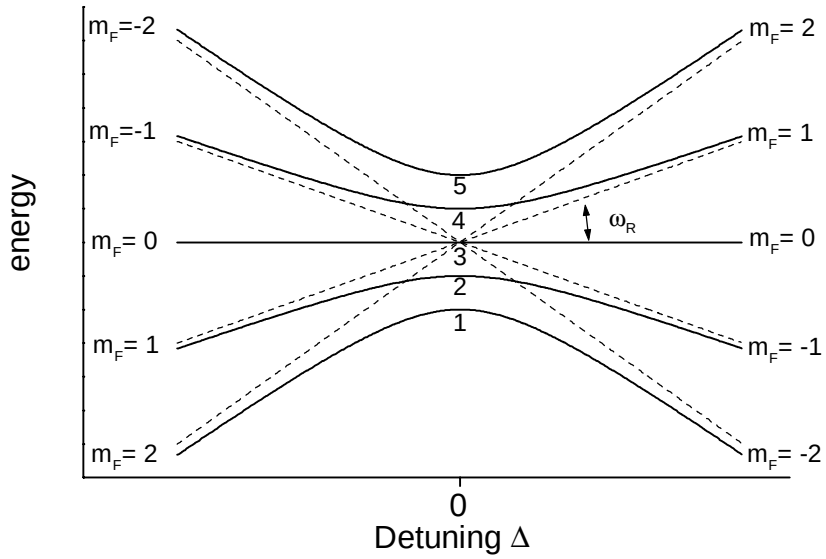

Figure 3.1: Eigenvalues of H^r as function of the detuning Δ. For reference, also the non perturbed eigenenergies are shown (dashed lines). Far of resonance the eigenstates coincide with the eigenstates of the non-interacting system, but near resonance the levels "repel" to form an "avoided crossing". The splitting between the energy levels equals ω_R.

a photon being either in the field or absorbed by the atom. Instead, the atom is said to be "dressed" with the photon energy. Eigenstates of H^r are therefore called "dressed states".

In this picture a transition from the trapped state to the untrapped state corresponds to an adiabatic passage along the eigenenergy curve. For a two level system and for a magnetic field varying linearly in time, the probability P that an atom passes adiabatically is given by the Landau-Zener formula $P = 1-e^{-2\pi\Gamma}$ [9], with Γ given by

$$\Gamma \equiv \frac{\omega_R^2}{\frac{d\Delta}{dt}}. \tag{3.14}$$

This parameter will appear naturally in our equations as we will see later on.

3.2.3 Interpretation

The Hamiltonian H^r defined in (3.12) is equivalent with the Hamiltonian of a spin in an effective magnetic field B_{eff} with a time varying component $\Delta(t)/\gamma$ in the z-direction and a static component ω_R/γ in the x-direction. This effective B-field is of magnitude $\sqrt{\Delta^2+\omega_R^2}/\gamma$ and its direction changes from the negative z-axis to the x-axis to the positive z-axis as the atom moves through resonance so that Δ changes its sign.

This system of a spin in a changing magnetic field behaves as the classical system of an angular momentum under influence of a changing external force. Initially, the spin will be precessing around the effective magnetic field axis with a frequency proportional to the magnitude of the effective field. As the direction of the effective magnetic field is changed slowly, allowing many cycles of the spin precession for a small change in direction of the field, the axis of the precession follows the axis of the effective magnetic field. So, as Δ changes sign, the spin is reversed (adiabatic passage). However, when the direction of the effective B-field is changed abruptly the axis of precession does not follow the axis of the field and the initial spin state remains unchanged (diabatic passage).

3.3 Evolution of the system

3.3.1 Time dependent Schrodinger equation

The time evolution of the state of the atom as the it moves through resonance is determined by the Schrödinger equation

$$i\frac{\partial}{\partial t}|\Psi^r(t)>=H^r(t)|\Psi^r(t)>. \tag{3.15}$$

We expand $|\Psi(t)>$ in the dressed state basis $|\phi_m(t)>$ as follows

$$|\Psi^r(t)>=\sum_m a_m(t)e^{-i\int^t \epsilon_m(t')dt'}|\phi_m(t)>, \tag{3.16}$$

with ϵ_m denoting the eigenvalues of H^r and where the unknown time dependent coefficients $a_m(t)$ are to be determined. Substituting the expansion (3.16) in the Schrödinger equation (3.15), using $H^r|\phi_n>=\epsilon_n|\phi_n>$ and multiplying both sides with $<\phi_n|$ from the left, we find a set of coupled differential equations for the coefficients a_n :

$$\frac{\partial}{\partial t}a_n(t)+\sum_m a_m(t)e^{i\int^t \epsilon_n(t')-\epsilon_m(t')dt'}<\phi_n(t)|\frac{\partial}{\partial t}\phi_m(t)>=0. \tag{3.17}$$

When the energy difference between two eigenstates is large, the factor $e^{i\int^t \epsilon_n(t')-\epsilon_m(t')dt'}$ will be quickly oscillating in time and so the coupling of these two eigenstates is surpressed. Only near resonance, when the difference in energy is minimum coupling can become significant.

3.3.2 Dimensionless variable

In order to facilitate numerical calculation and to gain more insight in the parameters governing the problem we introduce the dimensionless variable

$$z(t) \equiv \frac{\Delta(t)}{\omega_R}. \tag{3.18}$$

The new Hamiltonian as function of z and in units of $\hbar\omega_R$, is then given by

$$H^z(z) = -zF_z - F_x \tag{3.19}$$

and is implicitly dependent on the physical parameters $\omega_0(t)$ and ω_R of the system.

Substituting the new variable z in equation (3.17), a new set of equations is obtained for the new coefficients c_n, defined as $c_n(z(t)) \equiv a_n(t)$

$$\frac{\partial}{\partial z}c_n(z) + \sum_m c_m(z)e^{i\int^z \omega_R \frac{dt}{dz}(\epsilon_n(z') - \epsilon_m(z'))dz'} < \phi_n(z)|\frac{\partial}{\partial z}\phi_m(z) >= 0, \tag{3.20}$$

where the ϕ_n's and ϵ_n's are eigenvectors and eigenvalues respectively of H^z.

The equation thus obtained is only implicitly dependent on the real parameters of the system, such as the speed of passage, the form of the trap potential and the intensity of the rf-field. All these parameters are contained in the factor $\omega_R\frac{dt}{dz}$ appearing under the integral in the exponential. By definition (3.18) of z, we see that this factor is equivalent to the parameter Γ in eq. (3.14)

$$\omega_R\frac{dt}{dz} = \frac{\omega_R^2}{\frac{d\Delta}{dt}} \equiv \tilde{\Gamma}(z), \tag{3.21}$$

where the tilde symbol is used to stress that this "parameter" is actually a function of the dimensionless variable z. This function we will call the adiabaticity function. Only, when Δ is varying linearly in time, $\tilde{\Gamma}$ is a constant. In that case we will omit the tilde symbol and speak of the adiabaticity parameter.

3.3.3 The matrixelements $< \phi_n|\frac{\partial}{\partial z}\phi_m >$

Finally, we derive an analytical expression for the matrix elements $< \phi_n|\frac{\partial}{\partial z}\phi_m >$ appearing in (3.20). Taking the z-derivative of the equation $H^z|\phi_m >= \epsilon_m|\phi_m >$ and multiplying both sides from the left with $< \phi_n|$ one finds that for $m \neq n$ the matrix elements are given by

$$< \phi_n|\frac{\partial}{\partial z}\phi_m >_{n\neq m}= \frac{< \phi_n|\frac{\partial H^z}{\partial z}|\phi_m >}{\epsilon_m - \epsilon_n}. \tag{3.22}$$

For the case $m = n$ we use the fact that $|\phi_n >$ can always be chosen real (true for non-degenerate states) to show that

$$< \phi_n|\frac{\partial}{\partial z}\phi_n >= \frac{1}{2}\frac{\partial}{\partial z} < \phi_n|\phi_n >= 0, \tag{3.23}$$

see for example [**?**].

By diagonalization of H^z in the basis of the usual $|m_F>$ states and using the easy diagonal form of $\frac{\partial H^z}{\partial z}$, the quantities $\frac{<\phi_n|\frac{\partial H^z}{\partial z}|\phi_m>}{\epsilon_m-\epsilon_n}$ appearing in the right hand side of (3.22) can be analytically calculated.

After some analytic manipulation, a very simple form is obtained

$$<\phi_n|\frac{\partial}{\partial z}\phi_m>=\begin{pmatrix} 0 & 1 & 0 & 0 & 0 \\ -1 & 0 & \beta & 0 & 0 \\ 0 & -\beta & 0 & \beta & 0 \\ 0 & 0 & -\beta & 0 & 1 \\ 0 & 0 & 0 & -1 & 0 \end{pmatrix} \times \frac{1}{1+z^2}, \tag{3.24}$$

where $\beta \equiv \frac{<m_f=1|F_+|m_f=0>}{<m_f=2|F_+|m_f=1>} = \sqrt{\frac{3}{2}}$. The multiple zero entries of this matrix imply that only neighboring dressed states are coupled by the rf-field. Why this is the case is not yet clear.

3.4 Transition probabilities

Let's summarize the problem. We aim to calculate the probability of finding an atom, initially prepared in the trapped state $m_F = 2$, in an untrapped m_F state after it has moved through a region of resonance with the rf-field. This problem has been reduced to numerically solving the equations (3.20).

In the limit of large and negative z, the initial state of the atom $m_F = 2$ corresponds to the eigenstate $|\phi_1>$, where the dressed states $|\phi_m>$ are numbered from 1 to 5 by increasing eigenvalues as shown in figure 3.1. So, the boundary conditions for equation (3.20) are summarized as

$$\lim_{z\to-\infty} c_1(z) = 1 \text{ and } \lim_{z\to-\infty} c_{n\neq1}(z) = 0. \tag{3.25}$$

In the same way, the transition probability P to the untrapped m_F states $m_F = -2, -1, 0$ can be expressed as

$$P \equiv \lim_{z\to\infty} (|c_1(z)|^2 + |c_2(z)|^2 + |c_3(z)|^2). \tag{3.26}$$

For simplicity, let's assume that the adiabaticity function $\tilde{\Gamma}(z)$ is a constant:

$$\tilde{\Gamma}(z) = \Gamma. \tag{3.27}$$

The solutions of equations (3.20), and so the value of the transition probability P, are then purely determined by the value of Γ. A set of solutions $c_n(z)$ for $\Gamma = 0.1$ is shown in figure 3.2. The picture shows clearly how coupling between dressed states is surpressed for large and negative z, then becomes important in a region of resonance around $z = 0$ and then gets surpressed again for large z. For increasing Γ, the coupling between different dressed states is surpressed.

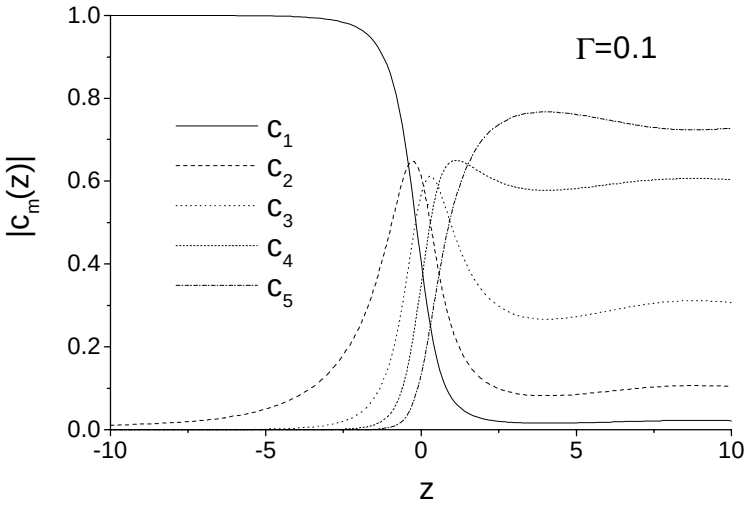

Figure 3.2: A set of solutions $c_n(z)$ for $\Gamma = 0.1$. Coupling between the dressed states is strong around the resonance $z = 0$.

This is shown in figure 3.3, where the coefficient $|c_1(z)|$ corresponding to the initial state $|\phi_1>$ of the atom, is plotted for different values of Γ. The transition probability to untrapped states P is calculated for different values of Γ as shown in figure 3.4. The value of P approaches unity around $\Gamma \sim 1$. At $\Gamma = 1$ the transition probability is: $P = 0.97$.

3.5 Rf-amplitude for efficient evaporative cooling

3.5.1 Lower bound

We first apply the results of the preceding section to calculate the minimum rf-amplitude $B_{\rm rf}$ needed in order to efficiently drive transitions to untrapped states. We consider the case of a Rubidium atom, trapped in the Ioffe trap described in chapter 2, passing a region of resonance with a constant velocity v in the outward radial direction in the plane of symmetry midway between the axial coils ($z = 0$). The magnetic field component of the rf-field is assumed to be directed perpendicular to the static trapping field.

The magnitude of the magnetic trapping field is found from equation (2.2)

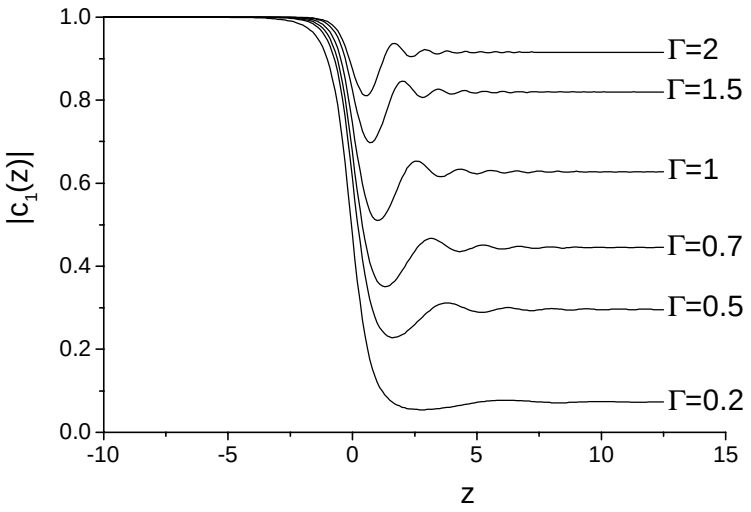

Figure 3.3: The solution $|c_1(z)|$ for different values of Γ. For increasing Γ coupling between dressed states is surpressed. For $\Gamma = 2$ the transition is almost completely adiabatic, while for $\Gamma = 0.2$ the transition is non-adiabatic.

as

$$\left|\vec{B}(\rho, z=0)\right| = \sqrt{a^2\rho^2 + B_0^2}, \tag{3.28}$$

with a the magnetic field gradient and B_0 the off-set field. As discussed in section 2, the magnetic field is effectively linear in ρ for temperatures $kT \gg U_0$ and for $kT \ll U_0$ it is harmonic, where $U_0 \equiv g_F m_F \mu_B B_0$. These two limits are separately discussed.

Linear limit

At the start of the cooling process the magnetic field is effectively linear in ρ: $B \approx a\rho$. Using the definition of the detuning Δ in equation (3.13), we find that the adiabaticity function $\tilde{\Gamma}(z)$ of (3.21) is a constant:

$$\tilde{\Gamma}(z) = \frac{\omega_R^2}{\frac{d\Delta}{dt}} = \frac{\omega_R^2}{\gamma \frac{dB}{d\rho}\frac{d\rho}{dt}} = \frac{\omega_R^2}{\gamma a v} = \Gamma \tag{3.29}$$

So, the result obtained in the preceding section can be directly applied to find the transition probability P for any given values of ω_R and v.

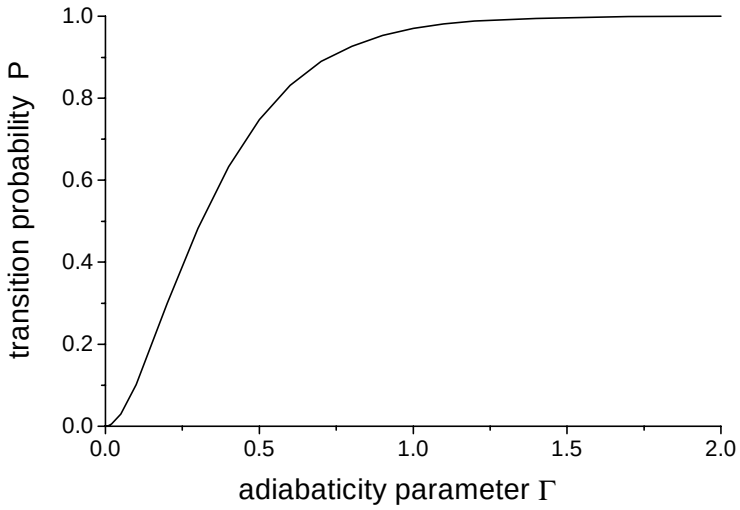

Figure 3.4: The transition probability to untrapped states P as function of the adiabaticity parameter Γ.

We assume the transition to be sufficiently saturated when the transition probability of an atom moving at twice the mean thermal velocity is close to unity. So we demand

$$P(\omega_R, 2v_T) \simeq 1. \tag{3.30}$$

with $v_T = \sqrt{\frac{8k_BT}{\pi m_{Rb}}}$ the mean thermal velocity of the Rubidium atom. Fixing $P(\omega_R, 2v_T)$ at 0.97, a value that is obtained for $\Gamma = 1$, we can express the amplitude of the rf-field needed in the evaporation process as a function of the temperature. For a temperature of $300\mu K$ in the beginning of the cooling process we find: $B_{\rm rf} = 1.3\ 10^{-5}$ Tesla. As temperature goes down, keeping the transition probability P constant, $B_{\rm rf}$ decreases as $\sqrt[4]{T}$.

Harmonic limit

For temperatures below $\sim 10\mu K$ the magnetic field at resonance is no longer linear. The magnetic field gradient will deviate from the value a in the linear limit and moreover, it will vary over the resonance region. However, when the resonance is considered to be sharp so that $\frac{dB}{d\rho}$ will not vary appreciably over the region of resonance, it is reasonable to approximate $\tilde{\Gamma}(z)$ by its value at the resonance $\tilde{\Gamma}(0)$. The effective adiabaticity $\Gamma_{\rm eff}$ thus introduced can be written

as the product of the adiabaticity parameter Γ in the linear case and a factor depending on the ratio of the truncation energy ε_t to the trapping parameter U_0:

$$\Gamma_{\text{eff}} = \tilde{\Gamma}(0) = \frac{\omega_R^2}{\gamma a v} \frac{1}{\sqrt{1 - (\frac{U_0}{U_0 + \epsilon_t})^2}} \tag{3.31}$$

The extra factor simply arises from the fact that the field gradient decreases as the position of resonance moves towards the field minimum. For high temperatures we have $\varepsilon_t \gg U_0$ and Γ_{eff} will approach the value of Γ in the linear limit given in (3.30).

The validity of this approximation can be easily checked by comparing the value of P calculated from the exact solutions of (3.20) with the values obtained using the constant Γ_{eff}. For $\Gamma_{\text{eff}} = 1$ we found that the error in the value of P is over the whole temperature range smaller than 0.1%.

The rf-field amplitude for a constant value of $\Gamma_{\text{eff}} = 1$ is shown as function of temperature in figure 3.5 for a constant truncation parameter $\eta = 8$. In the last stage of the cooling process at a temperature of $1\mu K$, the field amplitude B_{rf} has been reduced to $B_{\text{rf}} = 2.2\ 10^{-6}$ Tesla.

3.5.2 Upper bound

In order to have efficient evaporative cooling, the atoms of low energy in the center of the trap should not be affected by the rf-field. Therefore, we demand the mixing of the m_F states due to the interaction with the rf-field to be negligible for atoms near the trap center. From Hamiltonian (3.12) we find that this is the case when the detuning in the trap center $\Delta_0 \equiv |\Delta(\rho = 0, z = 0)|$ is large compared to ω_R:

$$\Delta_0 \gg \omega_R. \tag{3.32}$$

This condition yields an upper bound to the rf-amplitude.

The detuning in the trap center is related to the truncation energy as $\Delta_0 \equiv \omega_{\text{rf}} - \omega_0(\vec{r} = 0) = \frac{1}{2}\varepsilon_t/\hbar$, so condition 3.32 can be rewritten as

$$2\hbar\omega_R \ll \varepsilon_t.$$

The quantity $\hbar\omega_R$ appears in the dressed state picture as the splitting between the energy levels at the avoided crossing (see figure 3.1). Physically, this conditions states that the deformation of the trapping potential due to the rf-field should be small compared to the trap depth.

Here, we explicitly adopt the condition $2\hbar\omega_R < 0.1\varepsilon_t$ to find an upper bound to the rf-amplitude for efficient evaporative cooling. Both the upper and the lower bound are plotted in figure 3.5. At the start of the cooling process, the upper and lower bound are spaced far apart. The exact value of the rf-amplitude is not critical, as long as it is in between the two curves. For lower

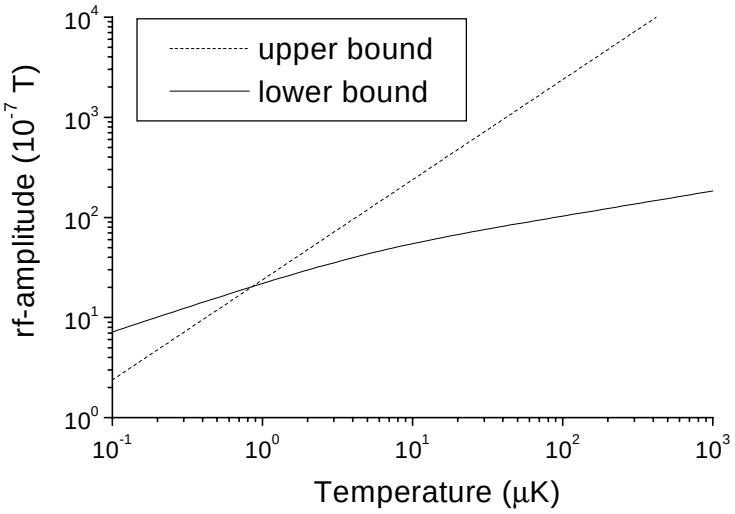

Figure 3.5: A lower bound and an upper bound to the rf-amplitude for efficient evaporative cooling. The lower bound originates from the condition that the rf-transition should be sufficiently saturated. The upper bound follows from the condition that the atoms in the trap center should not be affected by the rf-field. At a temperature $T \sim 1$ μK the lines cross, which implies that it may not be possible to efficiently remove the atoms with high energy from the trap without affecting the atoms with low energy in the center of the trap.

temperatures the spacing between the curves decreases and the lines even cross at a temperature $T \sim 1\mu K$. This implies that the exact value of the rf-amplitude is critical and that for very low temperatures it may not be possible to effectively remove atoms from the trap without affecting the atoms in the center of the trap.

3.6 Design of the rf-circuit

In the last section we calculated the amplitude of the rf-field needed for efficient cooling during the evaporation process. It depends on the temperature and on the truncation energy and necessarily decreases as the gas cools. In this section we discuss how this can be technically realized. Our aim is two-folded: First we aim for achieving an amplitude $B_{\mathrm{rf}} = 150{*}10^{-7}$ T at 50MHz, which corresponds to efficient evaporation at a temperature $T = 500\mu K$ for a truncation parameter $\eta = 10$. Then we must provide for a method to lower the rf-amplitude as the

temperature decreases.

3.6.1 Rf-coils

Coils of 1 mm thick copper wire of different number of windings N are tested ($N = 1, 2, 3, 4$). The dimensions of the coils are specified by the position at which they are fitted into the magnetic trap as discussed in section 2: The outer diameter $d = 31$mm and the outer edge of the coil can be placed 16mm from the atomic cloud. The wavelength of the electromagnetic wave at 50MHz is 6m, which is much larger than the dimensions of the coils. The self inductances L for the different coils are measured on an impedance analyzer (Hewlett Packard model 4192) at a frequency of 10MHz and are shown in the inset of figure 3.6. The coils are directly connected to an rf-generator without any impedance matching. The total impedance Z_{tot} is thus given by $Z_{\mathrm{tot}} = R_{\mathrm{int}} + i\omega L$, with R_{int} the internal resistance ($R_{\mathrm{int}} = 50\Omega$) of the rf-generator and ω the angular frequency. The output amplitude V_0 of the generator is set to $1 V_{\text{p-p}}$ into 50Ω.

The amplitude of the rf-field is measured using a pick-up coil of two windings of diameter 11mm (wirethickness 0.35 mm). Since the magnetic field is approximately homogeneous over the area of the small coil, the voltage over the pick-up coil V_{pu} is related to the oscillating magnetic flux as $V_{\mathrm{pu}} = n * A_{\mathrm{pu}} * \frac{dB}{dt}$, with $n = 2$ the number of windings and A_{pu} the area of the pick up coil ($A_{\mathrm{pu}} = 97$ mm^2). The field amplitudes measured in the coil center as a function of frequency are shown in figure 3.6. The solid lines are calculated from the currents through the rf-coils $|I| = |2V_0| / |Z_{\mathrm{tot}}|$ and using the well known formula for the B-field on the axis of a current loop

$$B(x) = \mu_0 I N \frac{r^2}{2(r^2 + x^2)^{3/2}}, \tag{3.33}$$

with r the coil radius ($r = 15$mm), x the distance from the coil center and μ_0 the vacuum permeability. The data points overlap with the calculated curves to a reasonable precision. The differences may be explained by the fact that the self inductance L is not constant over frequency range of interest. The coil with $N = 2$ produces the highest amplitude at 50MHz: $B_{\mathrm{rf}} = 6.2 * 10^{-7}$ T.

From this data we can obtain the power needed for the rf-generating system. Taking into account the decrease in amplitude of a factor 0.29 at a distance of 17 mm from the coil center (see 3.33), we find that an amplification of 38 dB is needed compared to the 1 $V_{\text{p-p}}$ setting of the function generator to obtain a field amplitude $B_{\mathrm{rf}} = 150 * 10^{-7}$ T. This corresponds to a maximum output power of the generating system of 17 Watt.

To investigate the influence of the magnetic trapping coils to the impedance of the rf-coil $N = 2$, the rf-amplitudes were measured with the rf-coil placed at its position in the magnetic trap. The results are shown in figure 3.7, where the measured and calculated rf-amplitudes from figure 3.6 for the coil $N = 2$ are shown for comparison. Apart from several small resonance peaks, the influence of the magnetic trap is mainly shown by the presence of a distinct resonance

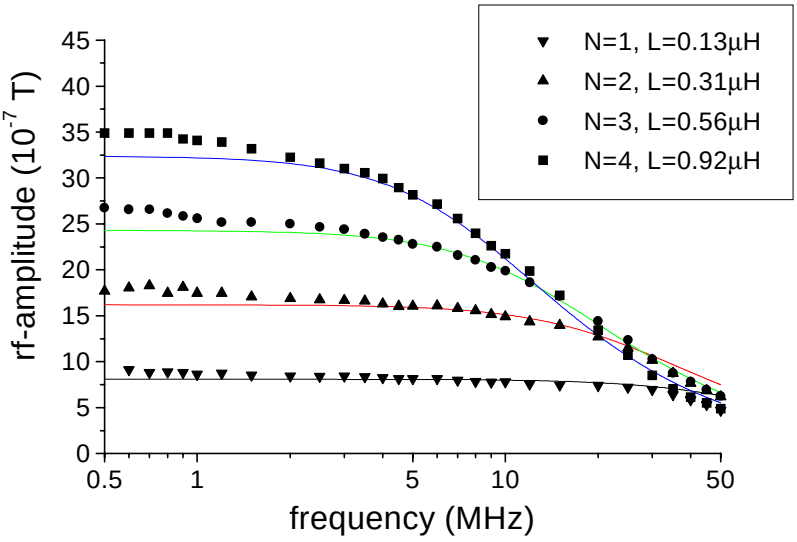

Figure 3.6: Rf-amplitudes measured in the coil center for coils of outer diameter $d = 31$ mm with different number of windings. The voltage of the rf-generator is set to 1 $V_{p\text{-}p}$. The amplitude of the rf-field is measured using a pick-up coil of two windings of diameter 11mm. The solid lines are calculated from the currents through the rf-coils $|I| = |2V_0| / |Z_{tot}|$ and using formula 3.33 for the B-field on the axis of a current loop

peak at 3 MHz. The width of the resonance, defined as the sum of the halfwidths of the upward peak and the downward peak, is ~ 0.4MHz. At the top of the resonance peak the amplitude is increased by a factor 3 and at bottom it is decreased by the same factor. The temperature corresponding to a rf-frequency of 3 MHz is ~ 30 μK (for $\eta = 8$). For this temperature the values for the upper and lower bound in figure 3.5 are spaced apart more than one order of magnitude.

3.6.2 Rf-Generator

In the final experimental set-up, the rf-field will be generated by a function generator (Wavetek model 80) that operates in the frequency range 10mHz to 50MHz. The frequency is controlled by supplying a voltage to the frequency modulation input. The rf-generator will be used in combination with a 25 Watt broadband RF Power Amplifier that operates over a frequency range 10kHz-250MHz. To decrease the rf-amplitude during the cooling process, a tunable attenuator was set up. The attenuation factor is tuned by a controller voltage.

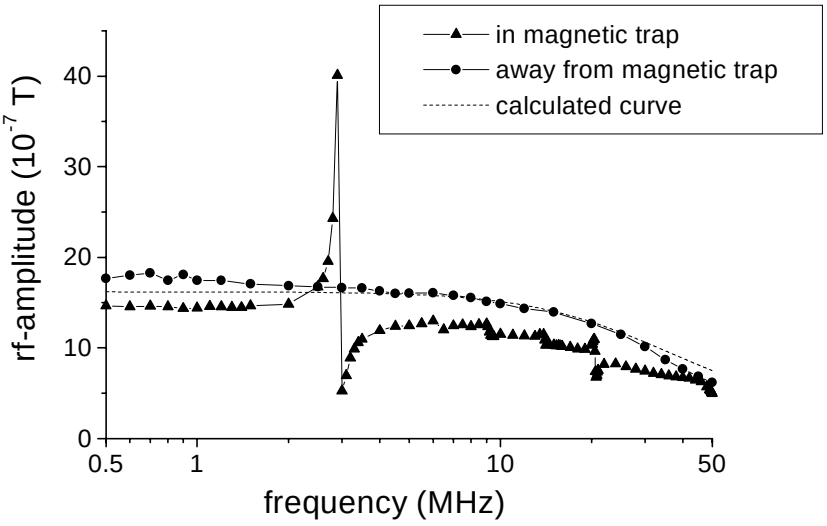

Figure 3.7: Rf-amplitudes measured for the coil $N = 2$ placed at its position in the magnetic trap. The measured and calculated rf-amplitudes from figure 3.6 for the coil $N = 2$ are shown for comparison. Apart from several small resonance peaks, the influence of the magnetic trap is mainly shown by the presence of a distinct resonance peak at 3 MHz. The width of the resonance, defined as the sum of the halfwidths of the upward peak and the downward peak, is ~ 0.4MHz. The rf-amplitudes at the top and the bottom of the resonance peak differ by a factor ~ 10.

In this way, the current through the rf-coil can be varied over $\sim$one order of magnitude over the frequency range of interest. Both the rf-frequency and amplitude are controlled by computer.

Chapter 4

Evaporative cooling

4.1 Introduction

Evaporation as a cooling mechanism is well known from daily life. It serves to carry off heat from the human body during exertion and cools a hot cup of coffee. The principle of evaporative cooling is based on the preferential removal of particles with an energy higher than the mean energy per particle and on thermalization by elastic collisions.

The same principle can be applied to cool trapped atomic gas samples. Let's assume that all atoms with an energy higher than a threshold value ε_t, the "truncation energy", will escape from the trap with unit probability. The truncation energy has to be chosen larger than the average energy per atom. By elastic collisions between atoms, the system tends to restore thermal equilibrium and to redistribute itself over all the available states. So, atoms are continuously scattered into the high-energy region ($\varepsilon > \varepsilon_t$) and leave the trap. Since these atoms carry away more than their share of mean energy the gas cools. This process is called plain evaporative cooling.

After a while the mean energy per remaining atom becomes much less than the truncation energy ε_t. As fewer and fewer atoms will acquire an energy sufficient to escape from the trap, the cooling will become less efficient and eventually be exponentially suppressed. To maintain a high cooling rate the truncation energy must be ramped down in time. We are now speaking of forced evaporative cooling. At this point it is convenient to introduce the truncation parameter η, which is defined as $\varepsilon_t = \eta kT$. Evaporative cooling with a constant truncation parameter is a typical example of "forced" evaporative cooling.

For the temperature regime of interest, elastic collisions result only from the s-wave channel. The elastic cross section σ is then only a function of the scattering length a and is for Bose atoms given by $\sigma = 8\pi a^2$. For ^{87}Rb in the $F = 2, m_F = 2$ state the scattering length can be found from [11] and yields $a = 109a_0$, with a_0 the Bohr radius.

In order for evaporative cooling to be efficient, an atom acquiring an energy

$\varepsilon > \varepsilon_t$ in an elastic collision event must leave the trap before experiencing another elastic collision. This will be the case when the mean free path λ is much larger than the dimension l of the sample:

$$\lambda \gg l. \tag{4.1}$$

At the start of the cooling process, at a typical density $n \sim 10^{12}$ cm^{-3} and temperature $T \sim 300$ μK, we have $\lambda = 1/n\sigma \simeq 0.5mm$ and the radial dimension $l \simeq kT/\alpha \simeq 0.1$ mm, with α the radial gradient of the magnetic potential (2.3). Thus condition (4.1) is satisfied. During the cooling process we may have to adiabatically expand the trap in order for this condition to remain satisfied.

4.2 Energy distribution function

Evaporation is by its very nature a non equilibrium process. Nevertheless, let's first briefly discuss some aspects of the energy distribution for a trapped atomic cloud in equilibrium in the non-degenerate regime. Applying Maxwell-Boltzmann statistics, as the classical limit of quantum statistics, one finds the Maxwell-Boltzmann (MB) energy distribution function

$$f(\epsilon) = ze^{-\varepsilon/kT}, \tag{4.2}$$

characterized by the temperature T of the atomic cloud. The fugacity z, also written in terms of the chemical potential μ as $z = e^{\mu/kT}$, follows from the condition

$$N = \int d\varepsilon \rho(\varepsilon) f(\varepsilon) \tag{4.3}$$

with N the number of atoms and $\rho(\varepsilon)$ the density of states. In the non-degenerate regime ($z \ll 1$) the fugacity can be expressed in terms of the particle density in the trap center and the thermal de Broglie wavelength $\Lambda = (2\pi\hbar^2/mkT)^{1/2}$ as

$$z = n(0)\Lambda^3, \tag{4.4}$$

where the quantity on the right side is called the phase-space density.

Now let's assume that all the atoms from the tail of the MB distribution (4.2) are removed. Since equilibrium is disturbed strictly speaking the temperature can not be defined. However, if the average energy per trapped atom is much smaller than the evaporation threshold, most interatomic collisions lead to a thermal redistribution of the energy over states in the range $\varepsilon < \varepsilon_t$. Therefore one may assume that the remaining atoms are in quasi equilibrium, distributed as a truncated MB distribution with a quasi-temperature T

$$f(\varepsilon) = ze^{-\varepsilon/kT} \times \Theta(\varepsilon_t - \varepsilon), \tag{4.5}$$

where $\Theta(\varepsilon_t - \varepsilon)$ is the Heaviside step function. The normalization constant z again follows from (4.3). When $\varepsilon_t \gg kT$ the parameters T and z reduce to the equilibrium temperature and fugacity respectively.

To assure that all atoms of energy $\varepsilon > \varepsilon_t$ leave the trap one must require "sufficient ergodicity". This means that the phase space distribution is only a function of the single-particle energy $\varepsilon(\mathbf{r}, \mathbf{p}) = p^2/2m + U(\mathbf{r})$. This allows us to write

$$f(\mathbf{r}, \mathbf{p}) = n_0 \Lambda^3 e^{-\varepsilon(\mathbf{r},\mathbf{p})/kT} \times \Theta(\varepsilon_t - \varepsilon(\mathbf{r}, \mathbf{p})). \tag{4.6}$$

Sufficient ergodicity is obtained in a trap with ergodic single particle motion [12]. If this is not the case we assume that the phase space distribution still obeys "sufficient ergodicity" as a result of interatomic collisions.

4.3 Modeling evaporative cooling

The process of evaporation can be described using the well known Boltzmann equation. Under conditions of sufficient ergodicity and assuming only s-wave collisions, the Boltzmann equation reduces to an equation for the evolution of the distribution function $f(\varepsilon)$ of a particularly simple form [13].

The group of Walraven showed by numerical solution of the Boltzmann equation that the evaporation process conserves the truncated MB distribution accurately. Subsequently, adopting the truncated MB distribution, analytical expressions were derived for the rate at which atoms are scattered into the high energy regime $\varepsilon > \varepsilon_t$ and for the energy they carry away on average. These expressions form the basis of a thermodynamical model describing the evaporation process [13],[14].

The most detailed modeling has been done numerically using the direct simulation Monte Carlo method [15] making no assumptions about the form of the distribution function at all. It can be used to study evaporative cooling in more complicated situations, for example when the elastic cross-section is energy dependent or when the mean free path of the atoms is comparable to the size of the gas cloud. However, the analytical treatment of Walraven gains more insight in the evaporation dynamics. In the following we will adopt the thermodynamical model of Walraven.

4.3.1 Thermodynamic properties

Partition function and reference volume

Once the truncated distribution (4.5) has been adopted a thermodynamical description of the atomic gas, analogous to the equilibrium case, follows naturally

with the truncation energy as an additional thermodynamic variable. As a starting point one writes for the normalization constant z in equation (4.5)

$$z \equiv n_0 \Lambda^3, \tag{4.7}$$

thus defining the reference density n_0 which, in the limit $\varepsilon_t \to \infty$, coincides with the density in trap center $n(0)$. From (4.3) it follows that the reference density can be expressed as

$$n_0 = \frac{N}{\zeta \Lambda^3}, \tag{4.8}$$

where we have defined the "truncated" partition function

$$\zeta = \int_0^{\varepsilon_t} d\varepsilon \rho(\varepsilon) e^{-\epsilon/kT}, \tag{4.9}$$

that is the ordinary partition function with truncated region $\varepsilon > \varepsilon_t$ left out. In analogy to the effective volume $V_{\text{eff}} = \frac{N}{n(0)}$, we can now define a reference volume V_e as

$$V_e \equiv \frac{N}{n_0} = \zeta \Lambda^3. \tag{4.10}$$

The reference volume has very nice properties due to its simple relation to the partition function. Therefore it is rather the reference volume V_e and the reference density n_0, instead of the true density in the trap center $n(0)$ and effective volume V_{eff}, that are introduced in the formalism.

The partition function ζ is a central quantity. In the case of power-law trapping potentials, characterized by the exponent δ and the constant A_{PL} defined in equation (2.6), it can be explicitly calculated:

$$\zeta_{PL} = A_{PL} \int_0^{\varepsilon_t} d\varepsilon \ \varepsilon^{1/2+\delta} e^{-\epsilon/kT} = \zeta_\infty P(3/2+\delta, \eta), \tag{4.11}$$

where $\zeta_\infty = A_{PL}(kT)^{3/2+\delta}\Gamma(3/2+\delta)$ is the partition function of an infinitely deep power law trap ($\eta \to \infty$) . The gamma function $\Gamma(a)$ and the incomplete gamma function $P(a, \eta)$ are defined as in [16]. It is seen that the partition function depends on the ratio of the truncation energy and temperature, i.e. on the truncation parameter η, explicitly.

Since the density of states in the Ioffe trap (2.7) is the sum of two power-law contributions, one easily finds for the partition function for the Ioffe trap

$$\zeta_{IQ} = \zeta_{PL}^{\delta=5/2} + \zeta_{PL}^{\delta=3/2}, \tag{4.12}$$

where the separate contributions $\zeta_{PL}^{\delta=5/2}$ and $\zeta_{PL}^{\delta=3/2}$ are found by substituting the indicated value of δ into equation (4.11). The associated constants $A_{PL}^{\delta=5/2}$

and $A_{PL}^{\delta=3/2}$ are determined by the trapping parameters α, β and U_0 in the Ioffe potential (2.3) as $A_{PL}^{\delta=5/2} = A_{IQ}$ and $A_{PL}^{\delta=3/2} = 2U_0 A_{IQ}$, where $A_{IQ} = (2m\pi^2)^{3/2}/[(2\pi\hbar)^3 2\alpha^2\beta^{1/2}]$ is defined in equation (2.7).

Density distribution

The density distribution is found by integrating the distribution function in phase space (4.6) over the momentum coordinates. The integral yields

$$n(\vec{r}) = \int d^3p f(\vec{r},\vec{p}) = n_0 \exp(-U(\vec{r})/kT) * P[3/2,\kappa], \tag{4.13}$$

with $\kappa(\vec{r}) \equiv (\varepsilon_t - U(\vec{r}))/kT$ [13] and $P(a,\eta)$ the incomplete gamma function [16]. In the limit of large η the truncated density distribution reduces to the equilibrium distribution $n(\vec{r}) = n(0)\exp(-U(\vec{r})/kT)$.

Energy

The total energy is obtained by counting the number of atoms in a state of energy ε, multiplying with their energy and summing over all states:

$$E = \int d\varepsilon\ \varepsilon\rho(\varepsilon)f(\varepsilon). \tag{4.14}$$

This can be expressed in terms of the logarithmic derivative of the partition function to temperature as

$$E = NkT\left(\frac{\partial \ln\zeta}{\partial \ln T}\right)_{\varepsilon_t}, \tag{4.15}$$

where the derivative is evaluated keeping the truncation energy constant. Using the definition of the reference volume (4.10), this expression can be rewritten in the form

$$E = (3/2+\gamma)NkT, \tag{4.16}$$

with

$$\gamma \equiv \left(\frac{\partial \ln V_e}{\partial \ln T}\right)_{\varepsilon_t}. \tag{4.17}$$

In the limit of large η the quantities $\frac{3}{2}NkT$ and γNkT can be interpreted as the kinetic and potential energy respectively. For finite η this is not the case, although their sum still is the total energy.

The parameter γ can be explicitly calculated for power-law traps using the expression (4.11) for the partition function:

$$3/2+\gamma_{PL} = \left(\frac{\partial \ln\zeta_{PL}}{\partial \ln T}\right)_{\varepsilon_t} = (3/2+\delta)R(3/2+\delta,\eta), \tag{4.18}$$

where $R(a,\eta) \equiv P(a+1,\eta)/P(a,\eta)$. Using the relation (4.12) for the partition function in the Ioffe, trap the parameter γ for the Ioffe trap can be written as a linear combination of γ_{PL}'s as

$$\gamma_{IQ} = \frac{\gamma_{PL}^{\delta=3/2} + c_{\mathrm{trap}}\ \gamma_{PL}^{\delta=5/2}}{1 + c_{\mathrm{trap}}}, \tag{4.19}$$

with $c_{\mathrm{trap}} \equiv \zeta_{PL}^{\delta=5/2}/\zeta_{PL}^{\delta=3/2} = (3kT/2U_0)R(3,\eta)$. In the high temperature limit $kT \gg U_0$ our γ_{IQ} reduces to $\gamma_{PL}^{\delta=5/2}$ and in the limit of low temperature $kT \ll U_0$ it reduces to $\gamma_{PL}^{\delta=3/2}$.

4.3.2 Kinetics

In the last section we have discussed some thermodynamical quantities in the case of a truncated MB distribution. Now let's discuss how the system evolves in the course of the evaporation process.

During the evaporation process particles are continuously lost from the trap, due to several distinct mechanisms. First of all particles leave trap due to evaporation. Secondly, particles are lost by "spilling". Spilling results from the fact that, as the truncation energy is ramped down, the atoms occupying states at the truncation edge of the MB distribution are simply "cut" away. Finally, particles are lost due to collisions with the background gas or by processes like dipolar relaxation and three-body recombination [17].

Summarizing, we write the rate of change of the number of trapped atoms as well as the rate of change of the total energy as the sums of the independent contributions of evaporation, spilling and loss mechanisms:

$$\dot{N} = \dot{N}_{ev} + \dot{N}_{spil} + \dot{N}_{loss}, \tag{4.20}$$

$$\dot{E} = \dot{E}_{ev} + \dot{E}_{spil} + \dot{E}_{loss}. \tag{4.21}$$

In this section these independent contributions will be discussed one by one.

Evaporation

By elastic collisions atoms may obtain an energy that is higher than the truncation energy and evaporate from the trap. This process is described by the Boltzmann equation. Under conditions of sufficient ergodicity and assuming only s-wave collisions, the Boltzmann equation reduces to an equation for the evolution of the distribution function $f(\varepsilon)$ of a particularly simple form [13]. The rate of change of the number of particles due to evaporation

$$\dot{N}_{\mathrm{ev}} = \int_{\varepsilon_t}^{\infty} \rho(\varepsilon)\dot{f}\,(\varepsilon)\,d\varepsilon \tag{4.22}$$

can then be expressed in terms of an evaporation volume $V_{\rm ev}$ as

$$\frac{\dot{N}_{\rm ev}}{N} = -n_0 \bar{v} \sigma e^{-\eta} \frac{V_{\rm ev}}{V_{\rm e}}, \tag{4.23}$$

with σ the cross-section for s-wave collisions and $\bar{v} \equiv \sqrt{8kT/\pi m}$ the mean thermal speed in equilibrium. The evaporation volume $V_{\rm ev}$, defined in [13], can be calculated as a function of temperature and truncation energy once the density of states is known. The ratio $V_{\rm ev}/V_e$ is for typical values of η between $5 \sim 10$ of the order unity. The evaporation rate (4.23) may be interpreted as the product of the elastic collision rate $n_0 \bar{v} \sigma$ and a probability that an elastic collision event produces an atom of energy higher than ε_t. This probability critically depends on η, because this parameter appears as an exponential in the equation.

The total energy loss due to the evaporation of atoms

$$\dot{E}_{\rm ev} = \int_{\varepsilon_t}^{\infty} \varepsilon \rho(\varepsilon) \dot{f}\,(\varepsilon)\, d\varepsilon \tag{4.24}$$

can be calculated introducing another volume $X_{\rm ev}$:

$$\dot{E}_{\rm ev} = \dot{N}_{\rm ev}[\eta + (1 - X_{\rm ev}/V_{\rm ev})]kT, \tag{4.25}$$

where the definition of the volume $X_{\rm ev}$ can be found in [13].The ratio $X_{\rm ev}/V_{\rm ev}$ depends only on the density of states in the trap and may vary between zero and one. Physically this means that the evaporating atoms carry away on average an energy less than kT above the truncation energy.

The evaporation volumes are explicitly calculated for power law traps. We have

$$V_{{\rm ev}PL} = \Lambda^3 \zeta_\infty [\eta P(3/2 + \delta, \eta) - (5/2 + \delta) P(5/2 + \delta, \eta)] \tag{4.26}$$

and

$$X_{{\rm ev}PL} = \Lambda^3 \zeta_\infty P(7/2 + \delta, \eta). \tag{4.27}$$

For the Ioffe trap, $V_{\rm ev}$ and $X_{\rm ev}$ may be expressed as the sums two power-law contributions:

$$V_{{\rm ev}IQ} = V_{{\rm ev}PL}^{\delta=3/2} + V_{{\rm ev}PL}^{\delta=5/2}, \tag{4.28}$$

and

$$X_{{\rm ev}IQ} = X_{{\rm ev}PL}^{\delta=3/2} + X_{{\rm ev}PL}^{\delta=5/2}. \tag{4.29}$$

Spilling

When the evaporation barrier is ramped down, atoms occupying states at the truncated edge of the truncated MB distribution are removed from the trap without contributing to the cooling of the sample. This is called spilling. Spilling may also occur due to other changes in the trap geometry, but here we consider only spilling due to the lowering of the truncation energy. The spilling rate is then given by the number of atoms occupying states near the truncated edge times the rate at which the truncation energy is ramped down:

$$\dot{N}_{\rm spil} = \rho(\varepsilon_t) f(\varepsilon_t) \dot{\varepsilon}_t. \tag{4.30}$$

Using the fact that $\rho(\varepsilon_t) f(\varepsilon_t) = n_0 \Lambda^3 \left(\frac{\partial \zeta}{\partial \varepsilon_t}\right)_T$ and using the definition (4.10) of the reference volume we obtain

$$\frac{\dot{N}_{\rm spil}}{N} = \xi \frac{\dot{\varepsilon}_t}{\varepsilon_t}, \tag{4.31}$$

where the spilling parameter ξ is defined by

$$\xi \equiv \left(\frac{\partial \ln V_e}{\partial \ln \varepsilon_t}\right)_T. \tag{4.32}$$

The energy loss rate is simply given by:

$$\dot{E}_{\rm spil} = \varepsilon_t \dot{N}_{\rm spil} \tag{4.33}$$

For power-law traps the spilling parameter ξ can be explicitly calculated,

$$\xi_{PL} = (3/2 + \delta)[1 - R(3/2 + \delta, \eta)], \tag{4.34}$$

and it is interesting to note that for power-law traps ξ is related to γ in a particularly simple way:

$$\gamma_{PL} + \xi_{PL} = \delta. \tag{4.35}$$

Similar to the expression for γ_{IQ} , we can write for the spilling parameter for the Ioffe trap

$$\xi_{IQ} = \frac{\xi_{PL}^{\delta=3/2} + c_{\rm trap} \xi_{PL}^{\delta=5/2}}{1 + c_{\rm trap}}, \tag{4.36}$$

from which we easily obtain

$$\gamma_{IQ} + \xi_{IQ} = \frac{3/2 + (5/2) c_{\rm trap}}{1 + c_{\rm trap}}. \tag{4.37}$$

Loss processes

In our atomic sample three kinds of collisions may contribute to atom loss. These are background collisions, two-body spin-relaxation and three-body recombination [17]. We may assume that all the products of such collisions leave the trap, either due to the fact that the product is in an untrapped state or because the recoil energy, that accompanies these collisions, makes the atom too energetic to be confined in the trap.

The rate of change of particles due to some i-body collision process is given by

$$\left(\dot{N}_{\rm loss}\right)_i = -\int d\mathbf{r} G_i(\mathbf{r}) n^i(\mathbf{r}), \tag{4.38}$$

with $G_i(\mathbf{r})$ the position dependent rate constant. Neglecting the position dependence of G_i, this expression can be written in the form

$$\left(\frac{\dot{N}_{\rm loss}}{N}\right)_i = -G_i n_0^{i-1} \frac{V_{ie}}{V_e}, \tag{4.39}$$

where we have introduced the reference volume for multibody collisions as

$$V_{ie} = \int d\mathbf{r} \left[\frac{n(\mathbf{r})}{n_0}\right]^i. \tag{4.40}$$

For two- and three-body collisions ($i = 2, i = 3$ resp.), this reference volume can be calculated numerically using the expression for the density (4.13). For background collisions ($i = 1$) this reference volume simply reduces to the ordinary reference volume introduced in (4.10).

The energy loss due to an i-body process can be written as

$$\left(\dot{E}_{\rm loss}\right)_i = \left(\dot{N}_{\rm loss}\right)_i \bar{\varepsilon}_i, \tag{4.41}$$

with $\bar{\varepsilon}_i$ the average energy of an escaping atom, that is given by:

$$\bar{\varepsilon}_i = \frac{\int d\mathbf{r} d\mathbf{p}\ n(\mathbf{r})^{i-1} f(\mathbf{r},\mathbf{p}) \varepsilon(\mathbf{r},\mathbf{p})}{\int d\mathbf{r} d\mathbf{p}\ n(\mathbf{r})^{i-1} f(\mathbf{r},\mathbf{p})}. \tag{4.42}$$

It can be shown that this expression can be rewritten as

$$\bar{\varepsilon}_i = (3/2 + \gamma_i) kT, \tag{4.43}$$

with

$$\gamma_i \equiv \frac{T}{i V_{ie}} \left(\frac{\partial V_{ie}}{\partial T}\right)_{\varepsilon_t}. \tag{4.44}$$

For background collisions we have $\gamma_1 = \gamma$, which implies that atoms that are removed by background collisions on average carry away an amount of energy

equal to the mean energy per atom, thus leaving the temperature of the sample unaffected. For two- and three-body collisions we have $\gamma_3 < \gamma_2 < \gamma$. Because these processes are more likely to occur in the trap center, where the density is the highest, the removed atoms carry away on average an amount of energy smaller than the mean energy per remaining atom. As a result these processes may cause heating of the sample.

4.3.3 Differential equations for the evolution of the gas

In the last sections we have discussed the processes that lead to particle and energy loss during evaporative cooling. From a thermodynamical point of view the decrease in energy is related to a change in the thermodynamical variables. Formally we can write:

$$\frac{dE(N,T,\eta)}{dt} = \left(\frac{\partial E}{\partial N}\right)_{T,\eta} \dot{N} + \left(\frac{\partial E}{\partial T}\right)_{N,\eta} \dot{T} + \left(\frac{\partial E}{\partial \eta}\right)_{N,T} \dot{\eta}. \tag{4.45}$$

The time derivative of the truncation parameter η is related to the time derivative of truncation energy and temperature as $\dot{\eta}/\eta = \dot{\varepsilon}_t/\varepsilon_t - \dot{T}/T$. Here, we have explicitly chosen η as the third thermodynamical variable, firstly because many thermodynamic quantities depend explicitly on η and secondly because we expect η to vary only slightly when the evaporation ramp is performed efficiently. Therefore, the term $(\partial E/\partial \eta)_{N,T}\,\dot{\eta}$ will be small and may for some purposes be neglected.

Having obtained explicit expressions for $\dot{N}$ and $\dot{E}$ in the preceding section, we see that expression (4.45) determines the time evolution of the quasi-temperature. Using equations (4.16) and (4.21), we rewrite (4.45) as

$$C_\eta \dot{T} = \dot{E}_{\mathrm{ev}} + \dot{E}_{\mathrm{spil}} + \dot{E}_{\mathrm{loss}} - (3/2+\gamma)\dot{N}kT - NkT\left(\frac{\partial \gamma}{\partial \eta}\right)_T \dot{\eta}, \tag{4.46}$$

where we have defined the heat capacity at constant η as

$$C_\eta \equiv \left(\frac{\partial E}{\partial T}\right)_{N,\eta} = [3/2 + \gamma + T\left(\frac{\partial \gamma}{\partial T}\right)_\eta]Nk. \tag{4.47}$$

Together with equation (4.20) we have now obtained a coupled set of equations describing the evolution of the quasi-temperature and the number of particles during the cooling process.

4.4 The efficiency of evaporative cooling

The aim of this thesis is, among others, to optimize the evaporation ramp. What do we mean by that ? It may be clear that, the higher we choose the truncation energy, the more energy each evaporating particle will carry away. In the extreme case we would put it almost at infinity and just wait for the

one particle containing all the energy of the sample to come along, achieving BEC at once. Off course this is a very speculative case: we would have to wait so long for this to happen that we would probably not live to see the event and moreover the sample would have since long vanished due to collisional loss. Therefore, we have to trade off between evaporation efficiency and evaporation speed to find the optimum value of the truncation energy.

In this section we will explain how to find this optimum value at any given instant in time with given values of N and T. Later on the results will be used to find the optimum trajectory of the truncation energy $\varepsilon_t(t)$.

4.4.1 The efficiency parameter

The efficiency of evaporative cooling is defined as the increase in phase-space density per particle loss. We formally define an efficiency parameter χ as

$$\chi \equiv -\frac{d\ln z}{d\ln N} = -\frac{\dot{z}/z}{\dot{N}/N}. \tag{4.48}$$

Since we obtained explicit expressions for the time derivatives of N and T in equations (4.20) and (4.46), it may be convenient to express the efficiency parameter χ in terms of the decrease in temperature per particle loss. So, we rewrite expression (4.48) as

$$\chi = -\frac{d\ln z(N,T,\eta)}{d\ln N} = -\left(\frac{\partial \ln z}{\partial \ln N}\right)_{T,\eta} - \left(\frac{\partial \ln z}{\partial \ln T}\right)_{N,\eta}\alpha - \left(\frac{\partial \ln z}{\partial \ln \eta}\right)_{N,T}\kappa, \tag{4.49}$$

with

$$\alpha \equiv \frac{d\ln T}{d\ln N} \tag{4.50}$$

and

$$\kappa \equiv \frac{d\ln \eta}{d\ln N}. \tag{4.51}$$

In the course of the cooling process we expect the number of particles in the trap to decrease about two orders of magnitude, while the truncation parameter should be approximately constant. So, unless sudden changes in the truncation parameter occur, we may expect the parameter κ to be much smaller than unity throughout the cooling process ($\kappa \ll 1$). Furthermore, reminding that $z = \frac{N}{V_e}\Lambda^3$, we have

$$\frac{\partial \ln z}{\partial \ln \eta} = -\left(\frac{\partial \ln V_e}{\partial \ln \eta}\right)_T = -\left(\frac{\partial \ln V_e}{\partial \ln \varepsilon_t}\right)_T \equiv -\xi, \tag{4.52}$$

which is much smaller than unity for typical values of η ($\xi \ll 1$). Therefore we may neglect the last term in expression (4.49) and write the efficiency parameter in terms of the parameters γ , ξ and α as

$$\chi = (3/2 + \gamma + \xi)\alpha - 1. \tag{4.53}$$

Since the quantity $(\gamma + \xi)$ for the Ioffe trap only slightly depends on η (and is constant in the case of a pure power-law trap) the η dependence of χ is primarily contained in the parameter α. Therefore, optimizing α automatically optimizes χ and from now on we consider simply the optimization of α.

The parameter α in the absence of loss processes

The parameter α is found by solving for $(\dot{T}/T)/(\dot{N}/N)$ in equation (4.46), while substituting $\dot{N}_{\rm ev} = \dot{N} - \dot{N}_{\rm spil} - \dot{N}_{\rm loss}$ for the evaporation rate. For the simplified case of evaporation in the absence of loss processes the parameter α can be written as

$$\alpha = \alpha_\eta - \kappa \frac{\xi(1 - X_{\rm ev}/V_{\rm ev}) + \eta \frac{\partial \gamma}{\partial \eta}}{C_\eta + \xi(1 - X_{\rm ev}/V_{\rm ev})}. \tag{4.54}$$

where

$$\alpha_\eta \equiv \left(\frac{d \ln T}{d \ln N} \right)_\eta = \frac{\eta + (1 - X_{\rm ev}/V_{\rm ev}) - (3/2 + \gamma)}{C_\eta/Nk + \xi(1 - X_{\rm ev}/V_{\rm ev})} \tag{4.55}$$

is the parameter α for evaporation at constant truncation parameter ($\kappa = 0$). Neglecting the term of the order κ in (4.54) ($\kappa \ll 1$), we have $\alpha \approx \alpha_\eta$. For power-law traps in the limit of large η, (4.55) reduces to

$$\alpha_\eta \simeq \frac{\eta - (3/2 + \delta)}{(3/2 + \delta)} \ (\eta \to \infty), \tag{4.56}$$

which shows that in the absence of collisions the efficiency parameter can be made arbitrarily large by choosing a large η .

4.4.2 The role of collisions

The presence of collisional loss sets a limit to the efficiency we may achieve. In order to have efficient evaporative cooling, substantially more atoms should be removed by evaporation than by background or inelastic collisions. Since the evaporation rate depends inversely exponential on η, this poses an upper limit to the truncation parameter for the evaporation process to dominate.

In this context we consider the ratio of evaporation rate to collision rate due to some i-body loss process, $R_i \equiv \dot{N}_{\rm ev}/\dot{N}_{\rm loss}$. From equations (4.23) and (4.39) we find

$$R_i = \frac{n_0 \bar{v} \sigma \frac{V_{\rm ev}}{V_e} e^{-\eta}}{n_0^{i-1} G_i \frac{V_{ie}}{V_e}} \equiv \frac{1}{\lambda_i} \frac{V_{\rm ev}}{V_e} e^{-\eta}, \tag{4.57}$$

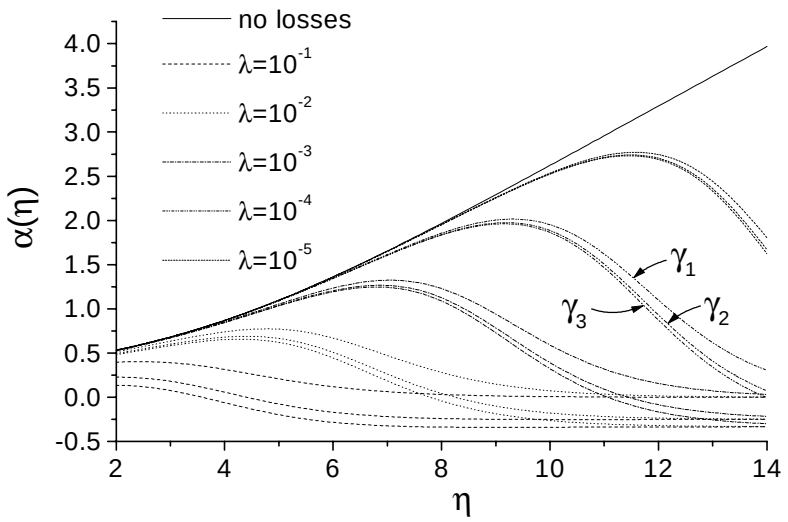

Figure 4.1: The efficiency parameter α in a harmonic trap as a function of the truncation parameter η for different values of the collision ratio λ, i.e. the ratio of the loss rate due to some i-body process and the elastic collision rate. Each value of λ corresponds to three curves, each curve corresponding to the case of only one-body (γ_1), two-body (γ_2) or three-body (γ_3) loss, where $\lambda_i = \lambda$. For decreasing λ, the maximum efficiency that may be achieved increases.

where we have defined the collision ratio λ_i as the ratio of the loss rate due to an i-body process to the elastic collision rate:

$$\lambda_i \equiv \frac{1/\tau_i}{1/\tau_{\rm el}} = \frac{n_0^{i-2} G_i}{\bar{v}\sigma} \frac{V_{ie}}{V_e}. \tag{4.58}$$

The quantity $1/\lambda_i$ is known as the ratio of good to bad collisions. In our equations we now substitute for the rate of change of particles

$$\dot{N}_{\rm ev} + \dot{N}_{\rm loss} = \dot{N}_{\rm ev}[1 + \sum_{i=1}^{i=3} R_i^{-1}] \tag{4.59}$$

and for the rate of change of energy

$$\dot{E}_{\rm ev} + \dot{E}_{\rm loss} = \dot{N}_{\rm ev}[\eta + (1 - X_{\rm ev}/V_{\rm ev}) + \sum\nolimits_{i=1}^{i=3} \frac{(3/2 + \gamma_i)}{R_i}]. \tag{4.60}$$

The parameter α in the presence of loss processes

For the parameter α at constant truncation parameter including loss processes, one finds

$$\alpha_\eta = \frac{\eta + (1 - X_{\rm ev}/V_{\rm ev}) - (3/2 + \gamma) - e^\eta \frac{V_{\rm ev}}{V_e} \sum_{i=2}^{i=3} (\gamma - \gamma_i)\lambda_i}{C_\eta/Nk + \xi(1 - X_{\rm ev}/V_{\rm ev}) + e^\eta \frac{V_{\rm ev}}{V_e} \sum_{i=1}^{i=3} [C_\eta + \xi(3/2 + \gamma_i - \eta)]\lambda_i}. \quad (4.61)$$

Compared to the expression (4.55) for α_η in the absence of losses, additional terms appear that depend exponentially on η. For the case of a harmonic trapping potential ($\delta = 3/2$), α_η is plotted as a function of η for different values of λ in figure 4.1. Each value of λ corresponds to three curves, each curve corresponding to the case of only one-body (γ_1), two-body (γ_2) or three-body (γ_3) loss, where $\lambda_i = \lambda$. For low values of η (i.e. $e^\eta \lambda \ll 1$) the terms originating from loss processes in (4.61) are negligible. For increasing values of η however, inevitably these terms will dominate ($e^\eta \lambda \gg 1$), causing α_η to decrease. The smaller λ, the higher is the efficiency that may be achieved.

Let's discuss what values of λ we may expect in practice. In accordance with previously performed experiments in other groups under similar vacuum conditions ($p \sim 10^{-11}$mbar), we expect the lifetime in the magnetic trap due to background collisions to be $\tau_{\rm bg} \sim 10$s. (see for example [18]). For the rate constant G_1 this yields $G_1 = 1/\ \tau_{\rm bg} = 0.1{\rm s}^{-1}$. The value of the rate constant G_2 for ^{87}Rb atoms in the $F = 2$, $m_F = 2$ state was obtained from [19]. This calculation predicts a slightly field dependent rate constant, that may be approximated, for the relevant field range 1-5 Gauss, by $G_2 \approx 9(2) * 10^{-15}$ cm^3/s.

For the rate constant for three-body recombination G_3, different values can be found in the literature. An analytical result was obtained by Fedichev et al.: The rate constant was expressed by in terms of the scattering length a as $G_3 = 3.9\hbar a^4/m$. For ^{87}Rb in the $F = 2$, $m_F = 2$ state we have $a = 109a_0$ [11] and thus $G_3 = 1.0 * 10^{-29}$ cm^6/s. A calculation on the basis of the Jastrow approximation, yielded $G_3 = 4 * 10^{-30}$cm^6/s [20]. Also measurements of G_3 have been performed. It has been determined for ^{87}Rb in the $F = 1$, $m_F = -1$ state in the non-degenerate gas ($G_3 = 4.3(1.8) * 10^{-29}$cm^6/s) as well as in the Bose Einstein condensate ($G_3^c = 5.8(1.9) * 10^{-30}$cm^6/s) [21]. For ^{87}Rb in the $F = 2$, $m_F = 2$ state in the condensate the rate constant was found to be $G_3^c = 1.8(1.9) * 10^{-29}$cm^6/s [18].

On the basis of the relation $G_3 \sim a^4$ one expects the rate constant for the |2,2> state to be a factor 2.4 higher than the rate constant for the |1,-1> state ($a = 109a_0, a = 88a_0$ [22] respectively). Therefore, we estimate the constant on the basis of the experimental value found for the |1,-1> state in the non-degenerate regime as $G_3 \approx 2.4 * 4.3(1.8) * 10^{-29} = 1.0(0.4) * 10^{-28}$ cm^6/s.

The collision ratio's λ_i from equation (4.57) are plotted in figure 4.2 as a function of density at a typical temperature of 10 μK. For changing temperature all the lines shift by the same small amount, due to the dependence of the elastic

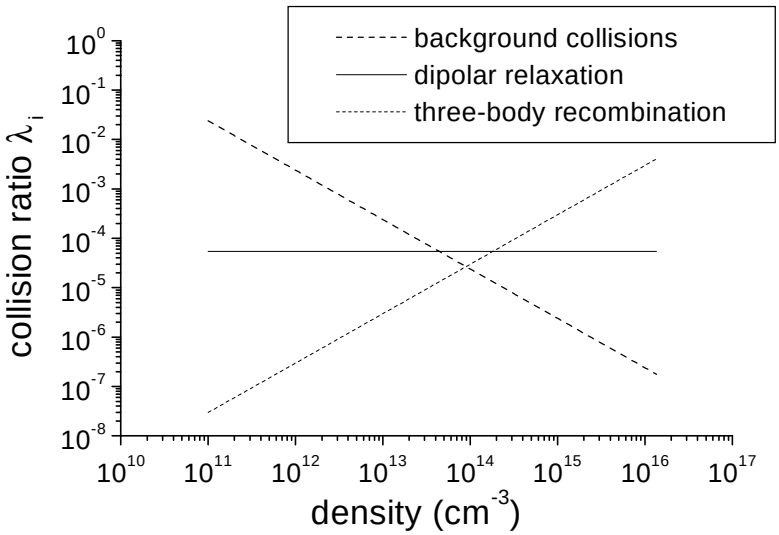

Figure 4.2: The collision ratio's λ_i of the loss rate to the elastic collision rate for several loss mechanisms, relevant for ^{87}Rb. The corresponding rate constants are: $G_1 = 0.1$ s^{-1}, $G_2 = 9 * 10^{-15}$ cm^3/s, $G_3 = 1 * 10^{28}$ cm^{-3}/s. For a density $n_0 \sim 9 * 10^{13}$, the dominant loss term originates from dipolar relaxation, for which $\lambda_2 \sim 10^{-4}$. In this density regime efficient evaporative cooling is assured.

collision rate to thermal speed ($\tau_{\rm el}^{-1} \sim \sqrt{T}$). From this picture it is very clear that for densities around $9 * 10^{13}$ cm^{-3} evaporative cooling can be extremely efficient. For $\lambda_2 \sim 10^{-4}$, we find from figure 4.1 that α_η may reach a value of 2. Substituting this value into equation (4.53) we find an efficiency $\chi = 5$.

4.4.3 Runaway evaporation

For a typical density $n_0 \sim 10^{12}$ cm^{-3} at the start of the cooling process, we see from figure 4.2 that the dominant loss term originates from background collisions. In this case, it is of vital importance that the elastic collision rate increases during the evaporation process. This will cause λ_1 to gradually decrease, making the process more and more efficient as it proceeds. This is known as run-away evaporation. The condition for run-away evaporation can formally be written as

$$\frac{d \ln n_0 T^{\frac{1}{2}}}{d \ln N} = 1 - (\gamma + \xi - 1/2)\alpha < 0. \qquad (4.62)$$

For a power-law trap with $\delta = 5/2$, which describes well the IQ trapping potential in the high temperature limit $kT \gg U_0$, this translates to a condition for α: $\alpha > 1/2$. From figure 4.1 we see that this can be easily achieved for an initial collision ratio $\lambda_{\mathrm{initial}} \lesssim 10^{-2}$. At a density $n_0 = 10^{12}$ cm^{-3} and temperature $T = 300$ μK, we find from (4.58) a minimum lifetime due to background collisions we can allow for:

$$\tau_{\mathrm{bg}} \gtrsim 1 \text{ s}. \tag{4.63}$$

When this condition is satisfied, the density may increases faster and faster as the evaporation process proceeds, making the cooling more and more efficient, until eventually the maximum efficiency is achieved at densities around $9 * 10^{13}$ cm^{-3}. Inevitably, the density continues to increase, now causing the efficiency to decrease, since three-body recombination has become the dominant loss mechanism. Adiabatic expansion of the trap may then be used to control the density, an issue that is discussed in section 4.6.

4.5 Simulation of the evaporative cooling process

The model developed in section 2.3, describes the evaporative cooling process by the equations (4.20) and (4.46) for the time evolution of the number of atoms N and the quasi-temperature T of the atomic cloud for a given trajectory $\eta(t)$ or $\varepsilon_t(t)$. In this section we will present numerical solutions of these equations. This will be done for the optimum trajectory $\eta(t)$, reaching the on-set of BEC with minimal particle loss, and for linear sweeps $\varepsilon_t(t) = \varepsilon_0 - a * t$ of the truncation energy. The results are expressed in phase diagrams $z(N)$, where the explicit time dependence $z(N(t), T(t), \eta(t))$ and $N(t)$ is omitted. Finally, we discuss the validity limitations of the model in the context of the experimental situation.

For numerically solving equations (4.20) and (4.46), we rewrite these equations in a dimensionless form. Dividing both sides of (4.20) by N and both sides of (4.46) by NkT, and further introducing the dimensionless time variable $\tau \equiv t/\tau_{\mathrm{ev}}$, where the evaporation time τ_{ev} is defined as

$$\tau_{\mathrm{ev}} \equiv -\left(\frac{\dot{N}_{\mathrm{ev}}}{N}\right)^{-1}, \tag{4.64}$$

we obtain the set of equations

$$\frac{\dot{N}}{N} = -[1 + \sum_{i=1}^{i=3} R_i^{-1}] + \xi[\frac{\dot{T}}{T} + \frac{\dot{\eta}}{\eta}], \tag{4.65}$$

$$\frac{C_\eta}{kN}\frac{\dot{T}}{T} = -[\eta + (1 - X_{\mathrm{ev}}/V_{\mathrm{ev}}) + \sum_{i=1}^{i=3} \frac{3/2 + \gamma_i}{R_i}] + \eta\xi[\frac{\dot{T}}{T} + \frac{\dot{\eta}}{\eta}] - (3/2 + \gamma)\frac{\dot{N}}{N} - \left(\frac{d\gamma}{d\eta}\right)_T \dot{\eta}, \tag{4.66}$$

where the dot denotes the derivative to τ. The quantities $\gamma, \xi, X_{\rm ev}/V_{\rm ev}, R_i$ and C_η appearing in the equations (4.65) and (4.66) are explicit functions of the thermodynamic variables N, T and η as discussed in the preceding sections. The quantity $\dot{\eta}/\eta$ may be replaced by $\dot{\varepsilon}_t/\varepsilon_t - \dot{T}/T$ (this follows directly from $\varepsilon_t = \eta k T$), depending on wether η or ε_t are specified functions of time.

4.5.1 Optimized trajectories through phase-space

In order to find the optimized trajectory through phase space one should consider the exact expression (4.49) for the efficiency parameter χ, a function of the number of particles N, the temperature T, the truncation parameter η and of the rate of change of the truncation parameter $\dot{\eta}$, to minimize the total particle loss as the degeneracy parameter increases from its initial value z_0 to the value at the BEC on-set z_{BEC}. Formally, one should minimize the function

$$\Delta \ln N = \int_{\ln z_0}^{\ln z_{BEC}} \chi^{-1}(N, T, \eta, \dot{\eta}) d \ln z, \tag{4.67}$$

under variation of the entire trajectory $\eta(t)$.

One may assume that for any optimized trajectory $\eta(t)$ the truncation parameter varies only slightly compared to variations in the number of particles, i.e. $\kappa \equiv \frac{d \ln \eta}{d \ln N} \ll 1$. This allows us to neglect the contribution of the variation of η in the efficiency parameter χ. Then the rather complex problem of minimizing (4.67) reduces to minimizing

$$\Delta \ln N \approx \int_{\ln z_0}^{\ln z_{BEC}} \chi_\eta^{-1}(N, T, \eta) d \ln z, \tag{4.68}$$

with $\chi_\eta \equiv (3/2 + \gamma + \xi)\alpha_\eta - 1$ and α_η given by expression (4.61).

Minimizing the integral in (4.68) was done by optimizing the parameter α_η at every time step, using a simple numerical optimization scheme: 1) An initial optimal value $\eta^1_{\rm max}$ is found from the maximum of the parameter α_η at the initial values of the number of atoms and temperature N_1 and T_1 . 2) The equations are solved for a small interval in the evaporation time, keeping $\eta = \eta^1_{\rm max}$ constant. 3) The final values N_2 and T_2 are substituted into α_η to find an optimum value of the truncation parameter $\eta = \eta^2_{\rm max}$. 4) The equations are solved for the same time interval, now with η varying linearly from $\eta^1_{\rm max}$ to $\eta^2_{\rm max}$. Steps 3) and 4) are repeated until the value of $\eta^2_{\rm max}$ has converged to some specified precision. This routine is performed for successive time intervals until the degeneracy parameter $z = n_0 \Lambda^3$ has reached the value of 2.6. For our case, using a time interval $\Delta\tau = 0.1$, the on-set of BEC was reached in about 20 intervals. We should stress that, although the trajectories are continued up to the BEC transition point, the model does not include degeneracy effects and is thus only valid for $z \ll 1$.

If the state of the thermodynamic system would be entirely specified by N and z (or by N and T), then the approach of instantaneously optimizing

the parameter χ_η to minimize the integral in (4.68) would be exact. This can be understood by considering the phase-space density produced by the instantaneously optimized trajectory $z_{\rm inst}(N)$ and that of an alternative trajectory $z_{\rm alt}(N)$. Since $z_{\rm inst}$ is optimized at the beginning of the trajectory, initially $\Delta N_{\rm alt} > \Delta N_{\rm inst}$ for a given increase in z. If finally $\Delta N_{\rm alt} < \Delta N_{\rm inst}$ at the on-set of BEC, then the two trajectories must have crossed. This can only occur if for some value of N

$$-\frac{dz_{\rm alt}(N)}{dN} > -\frac{dz_{\rm inst}(N)}{dN}, \tag{4.69}$$

which is impossible by the construction of $z_{\rm inst}(N)$. So, $z_{\rm inst}(N)$ represents the optimum trajectory [23]. As the state of the thermodynamic system does not depend on N and z alone, but also on the truncation parameter η, this argument strictly spoken doesn't apply. However, since thermodynamic quantities depend only slightly on η , the trajectory $z_{\rm inst}(N)$ minimizes (4.68) to a good approximation.

The trajectories $z(N)$ optimized for minimum particle loss using the numerical scheme described above, are shown in figure 4.3 for different starting values N_0 of the number of atoms. The corresponding trajectories $\varepsilon_t(t)$ are shown in figure 4.4. For a large initial number of atoms $N_0 \sim 10^{10}$ the starting density is of the order 10^{13} cm^{-3} for the trapping conditions described in chapter 2. This allows very efficient cooling ($\chi \sim 5$), which shows from the steepness of the curve. As the system approaches the BEC onset, the efficiency decreases due to rapid loss from three body collisions. The on-set of BEC is reached at $T \sim 4$ μK and $n_0 \sim 3 * 10^{15}$ cm^{-3}, which yields for the collision ratio $\lambda_3 \sim 2 * 10^{-3}$. Due to the conditions of high density, the evaporation process is fast; the BEC on-set is reached in about 0.5 s. For $N_0 = 10^9$, the overall efficiency is the highest: $\chi_{\rm tot} \equiv -\Delta \ln z / \Delta \ln N = 3.8$. The BEC on-set is reached at a density $n_0 \sim 1 * 10^{15}$ cm^{-3} at a temperature $T \sim 2$ μK and the evaporation ramp takes about 2s. For $N_0 = 1 * 10^8$ cm^{-3}, the final values for density and temperature are: $n_0 \sim 1 * 10^{14}$ cm^{-3}, $T \sim 0.5$ μK for an evaporation ramp of 7 s.

When the leading loss term is background collisions, run-away evaporative cooling manifests itself in an upward curving trajectory in phase-space. The importance of run-away evaporation is nicely illustrated by the two trajectories outermost to the left in figure 4.3. At $N_0 = 2 * 10^7$ the collision ratio λ_1 is just above the value allowed for run-away evaporation, while at $N_0 = 3 * 10^7$ the collision ratio λ_1 is just below this value. The difference in the phase space density that may finally be achieved is dramatic.

In general the optimized trajectories $\varepsilon_t(t)$ are of different shape and can not be characterized by some specific form. One might say that when the leading loss term is background collisions, the trajectories are of exponential form. However, for an initial number of atoms $N_0 = 10^9$ the trajectory is to a good approximation linear and for $N_0 > 10^9$ the optimum trajectories are curving downward.

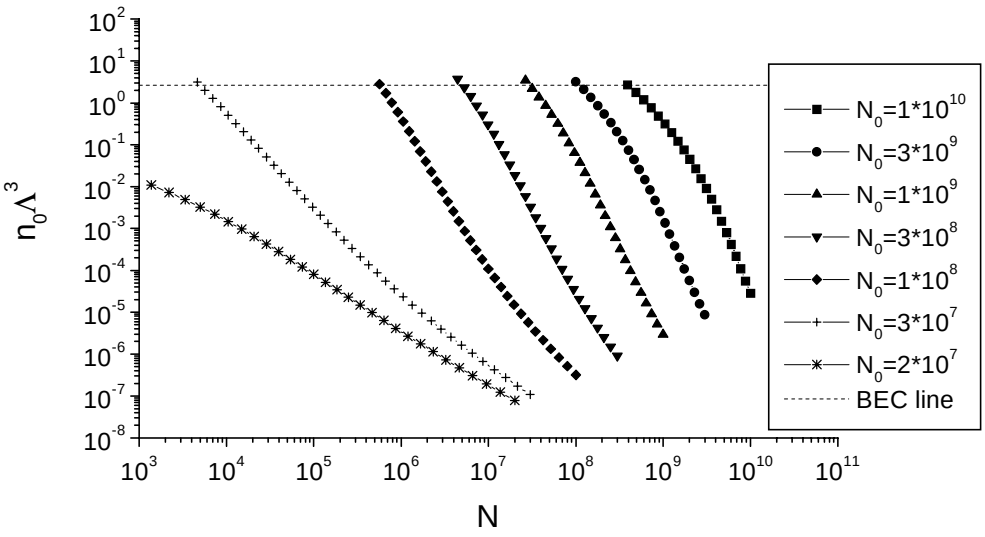

Figure 4.3: Optimized trajectories through phase- space for the Ioffe trap for different starting values of the number of atoms N_0. The initial temperature is $300\mu K$ in each case. The trapping potential is of the form **??** with trapping parameters $a = 3.77$ T/m, $b = 162\mathrm{T/m}^2$ and $B_0 = 10^{-4}$T. The loss rate due to background collisions $G_1 = (10\mathrm{s.})^{-1}$, the two-body rate constant $G_2 = 9 * 10^{-15}\mathrm{cm}^3/\mathrm{s}$. and the three-body rate constant $G_3 = 1 * 10^{-28}\mathrm{cm}^6/\mathrm{s}$. The elastic crossection for ^{87}Rb in the $F = 2$, $m_F = 2$ state $\sigma = 8.5 * 10^{-12}$ cm^2. The points correspond to equal intervals in evaporation time $\Delta\tau = 0.1$.

For typical experimental conditions $N_0 = 10^9$ the trajectories through phase-space corresponding to a linearly decreasing truncation energy are shown in figure 4.5. The initial value of the truncation energy $\varepsilon_t(0)$ corresponds to the initial optimum value of η and the slopes a are varied. Over a large range in a the resulting trajectories through phase space are very close to the optimal curve. The evolution of the temperature in response to the variation of the truncation energy is such, that the truncation parameter remains close to its optimal value. This effect is only seen for the optimized curve for starting value $N_0 = 10^9$.

4.5.2 Applicability of the model and experimental realization

The optimized curves look promising, in regard to the number of atoms we should be able to condense. Assuming an initial number of atoms $N_0 = 10^9$, the

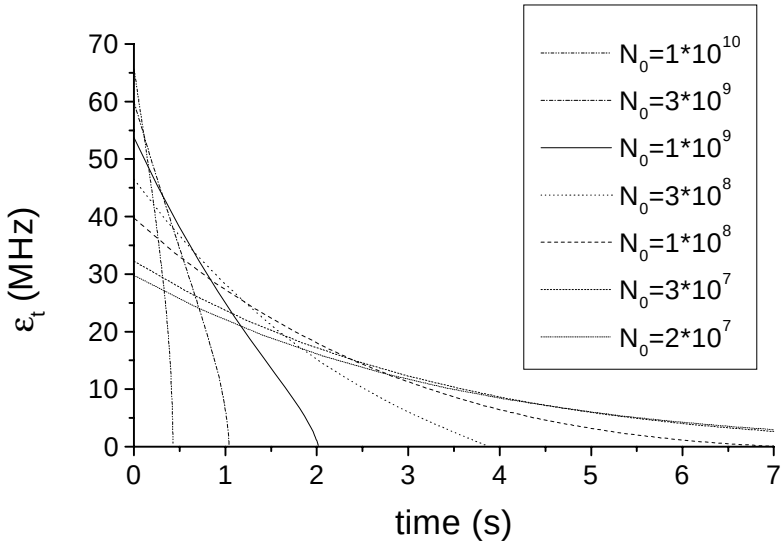

Figure 4.4: Optimum trajectories $\varepsilon_t(t)$ corresponding to the optimized trajectories through phase space in figure 4.3. The optimized evaporation ramps for $N_0 = 2 * 10^7$ and $N_0 = 3 * 10^7$ are only shown up to 7 seconds. The corresponding curves in figure 4.3 represent evaporation ramps of 20 and 16 seconds respectively.

simulation predicts that the on-set of BEC can be reached with more than 10^7 atoms remaining. This is much more than was obtained in previous BEC experiments with ^{87}Rb, see for example [5]. However, we should make some critical remarks concerning the experimental realization of the optimized evaporation ramps and the applicability of the model. This will be done explicitly for the optimized trajectory with $N_0 = 10^9$.

The first remark concerns condition (4.1), stating that for evaporation to be efficient, the mean free path of an atom should be much larger than the dimension of the sample. For the final density $n_0 \sim 1 * 10^{15}$ cm^{-3} we find for the mean free path $\lambda = 1/n_0\sigma \simeq 1$ μm, and at a temperature $T \sim 2$ μK we find for the radial dimension $l = \sqrt{kT/(\alpha^2/2U_0)} \simeq 6$ μm. Clearly condition (4.1) is not satisfied. So, we may expect cooling to be less efficient than the numerical simulation predicts.

Secondly, let's consider the lifetime of our sample at the BEC on-set. This

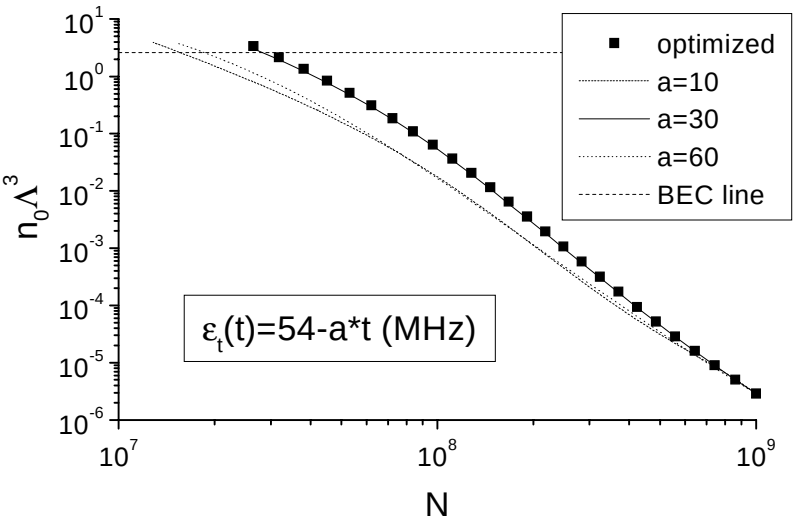

Figure 4.5: Trajectories through phase space for a linearly decreasing truncation energy with different slopes a. The initial number of atoms $N_0 = 10^9$ and the initial temperature $T = 300$ μK. Over a wide range in a the trajectories are close to the optimum trajectory.

is determined by the three-body collision rate (4.39) as

$$\tau_{3\mathrm{B}} = -\left(\frac{\dot{N}_{3B}}{N}\right)^{-1} = \left(G_3 n_0^2 \frac{V_{3\mathrm{e}}}{V_e}\right)^{-1}. \tag{4.70}$$

Substituting the final density and using $\frac{V_{3e}}{V_e}(\eta \to \infty) = 0.2$ we find $\tau_{3\mathrm{B}} \simeq 50$ms. This lifetime is not sufficient for performing experiments with the condensate.

A third remark concerns the time scale of the evaporation. In spite of the very short lifetime of the sample, the collision ratio $\lambda_3 \sim 10^{-3}$ poses no serious restrictions to the efficiency of the evaporation process under the condition that the evaporation speed is very high. More precisely, for the optimized curve $N_0 = 10^9$, the final interval in the dimensionless time $\Delta\tau = 0.1$ corresponds to a true time interval $\Delta t \simeq 1$ms. In order for the model to be applicable to the true experimental situation, the truncation energy, i.e. the rf-frequency, should be smoothly varying on this time scale. This is not the case for our experimental set-up.

All three problems discussed above are directly related to the high densities ($\gtrsim 10^{14}$ cm^{-3}) that are inevitably reached when many atoms are contained in a tight trapping potential at a phase-space density near the on-set of BEC. There-

fore, adiabatic expansion of the magnetic trapping potential may be performed in the final stage of the cooling process.

4.6 Adiabatic expansion of the trapping potential

As we have seen in the preceding section, several problems are encountered when the density of the atomic gas sample rises above $\sim 10^{14}$ cm^{-3}. These problems might be circumvented by adiabatically expanding the trapping potential. Adiabatic expansion trades in density for temperature, keeping the phase-space density constant. In this section we will give a short discussion of the scaling of density and temperature with the trapping parameters α, β and U_0, and describe how an adiabatic change of the trapping parameters affects spilling in the evaporation process. Since adiabatic expansion is only relevant at low temperatures, we treat the case of a purely harmonic trapping potential as the limiting case $kT \ll U_0$ of the Ioffe trapping potential.

The reference density in the limit $\eta \to \infty$ is found from definition (4.7)

$$n_0 \simeq \frac{N}{\Lambda^{3/2}\zeta_\infty^{\delta=3/2}} = N f(\theta)(kT)^{-3/2}, \tag{4.71}$$

with $\zeta_\infty^{\delta=3/2} = 2U_0 A_{IQ}(kT)^3\Gamma(3)$ the partition function of an infinitely deep Ioffe trap in the harmonic limit $kT \ll U_0$. Here, A_{IQ} is given in (2.7). The set of trapping parameters $\{\alpha, \beta, U_0\}$, that we denote by θ, is contained in the function

$$f(\theta) = \frac{1}{2\pi^{3/2}} \frac{\alpha^2\beta^{1/2}}{U_0}.$$

For an adiabatic change in one of the trapping parameters, phase-space density is conserved and so $T \sim (n_0)^{2/3}$ during expansion. From (4.71) we then find that the density scales as

$$n_0 \sim \sqrt{f(\theta)}. \tag{4.72}$$

In particular, for a variation of the radial gradient α, the density scales as

$$n_0 \sim \alpha. \tag{4.73}$$

and the temperature

$$T \sim \alpha^{2/3}. \tag{4.74}$$

In regard to condition (4.1), we find that the mean free path λ scales as $\lambda \sim \alpha^{-1}$ and that the radial dimension of the sample $l \sim \alpha^{-2/3}$.

The parameter α can be decreased in a controlled way over several orders of magnitude by decreasing the current through the Ioffe bars (see section 2.2). On the basis of the scaling relation (4.73) we find that this is an effective method to increase the lifetime of the sample at the BEC onset and to control the speed of the cooling process. Further, it slightly improves the ratio of the mean free path and the radial dimension of the sample.

An additional advantage of adiabatic expansion is a small reduction of the spilling rate. The spilling of atoms for general trap changes can be derived from the total number of quantum states Ω available [24]. In the limit of harmonic trapping potential, the density of states $\rho(\varepsilon) \approx 2U_0 A_{IQ} \varepsilon^2$ and so

$$\Omega(\varepsilon_t, \theta) = \int_0^{\varepsilon_t} d\varepsilon \ \rho(\varepsilon) = \frac{2}{3} U_0 A_{IQ} \varepsilon_t^3. \tag{4.75}$$

The rate of change of number of atoms due to spilling is given as

$$\dot{N}_{\text{spil}} = f(\varepsilon_t)\dot{\Omega} = f(\varepsilon_t)(\frac{\partial \Omega}{\partial \varepsilon_t}\dot{\varepsilon}_t + \frac{\partial \Omega}{\partial \theta}\dot{\theta}). \tag{4.76}$$

Let's again consider the case of adiabatic expansion by reducing the radial gradient α. Using $\frac{\partial \Omega}{\partial \alpha} = -2\frac{\Omega}{\alpha}$ (since $A_{IQ} \sim \alpha^{-2}$) and further $\frac{\Omega}{\varepsilon_t \rho(\varepsilon_t)} = 1/3$, the spilling rate can be written as the product of the spilling rate for constant trap parameters (4.31) and a factor that depends on the ratio of the rate of change of α and the rate of change of ε_t :

$$\frac{\dot{N}_{\text{spil}}}{N} = \xi \frac{\dot{\varepsilon}_t}{\varepsilon_t}(1 - \frac{2}{3}\frac{\dot{\alpha}/\alpha}{\dot{\varepsilon}_t/\varepsilon_t}). \tag{4.77}$$

So, when $\dot{\alpha}/\alpha$ is of the order $\dot{\varepsilon}_t/\varepsilon_t$ the spilling rate can be significantly reduced.

However, for high values of the truncation parameter $\eta \sim 8$, particle loss due to spilling is much smaller than the particle loss due to evaporation. For example, for the optimized curve with $N_0 = 10^9$ in figure 4.3, particle loss due to spilling is only a factor ~ 1.6. Therefore, the reduction of the spilling rate will not be of great significance to the efficiency of the cooling process.

4.7 The dimensionality of evaporation

In the discussion of evaporative cooling we have always considered ideal evaporation. In particular, we assumed that the selection criterion for the removal of atoms was based on the total energy ε of the atom. However, for real experiments this is not always the case.

In this context we introduce the notion "effective dimension of evaporation". If the selection criterion for removal of atoms is based on the total energy, i.e. $\varepsilon > \varepsilon_t$, evaporation is said to be three dimensional (3D). However, if this criterion is based on the energy for the motion in one or two particular directions, i.e.

$\varepsilon_x > \varepsilon_t$ or $\varepsilon_x + \varepsilon_y > \varepsilon_t$, evaporation is called one respectively two dimensional. The efficiency of 1D evaporation is much less compared to 3D evaporation due to a drastic decrease in the evaporation rate by a factor $\sim 4\eta$ [12].

Since the evaporation surface, determined by the resonance condition (3.1), entirely encloses the atomic sample, rf-induced evaporation in the Ioffe trap is in principle a 3D evaporation scheme. However, due to the gravitation potential, the evaporation may become effectively one dimensional.

Taking into account gravitation, the total potential is no longer symmetric in ρ. In particular, in the horizontal radial direction the potential energy is given by

$$V_{\mathrm{hor}}(\rho) = V_B(\rho, 0), \tag{4.78}$$

with $V_B(\rho, z)$ the magnetic potential (2.3), while in the vertical radial direction one must take into account also the gravitational potential

$$V_{\mathrm{ver}}(\rho) = V_B(\rho, 0) + m_{\mathrm{rb}} g \rho, \tag{4.79}$$

with g the acceleration of gravity. The difference in potential energy ΔV in the horizontal and vertical direction at the evaporation surface is thus given by

$$\Delta V = m_{\mathrm{rb}} g \rho_{\mathrm{res}}, \tag{4.80}$$

with ρ_{res} determined by the resonance condition (3.1).

Evaporation is most likely to occur at the bottom of the evaporation surface, where the effective evaporation barrier is ΔV lower than the evaporation barrier to the sides of the surface. When ΔV is much larger than kT, evaporation in other directions than the vertical direction are ruled out and the evaporation will be effectively one dimensional. The condition for 3D evaporation

$$\Delta V \ll kT \tag{4.81}$$

will now be discussed for the limit $kT \gg U_0$ of linear radial potential and for the limit $kT \ll U_0$ of harmonic radial potential separately.

Linear limit

For high temperatures the magnetic potential reduces to $V_B(\rho, 0) \approx \alpha\rho$, as shown in figure 4.6. The resonance position ρ_{res} can be written as $\rho_{\mathrm{res}} = \varepsilon_t/\alpha$, with ε_t the truncation energy assuming gravitation is absent. Condition (4.81) now reads

$$\Delta V = \frac{m_{\mathrm{rb}} g}{\alpha} \varepsilon_t \ll kT,$$

from which a condition for the truncation parameter η can be derived:

$$\eta \ll \frac{\alpha}{m_{\mathrm{rb}} g} = 25. \tag{4.82}$$

As η typically varies between $5 \sim 10$, evaporation can be considered to be three dimensional in the limit of linear radial trapping potential.

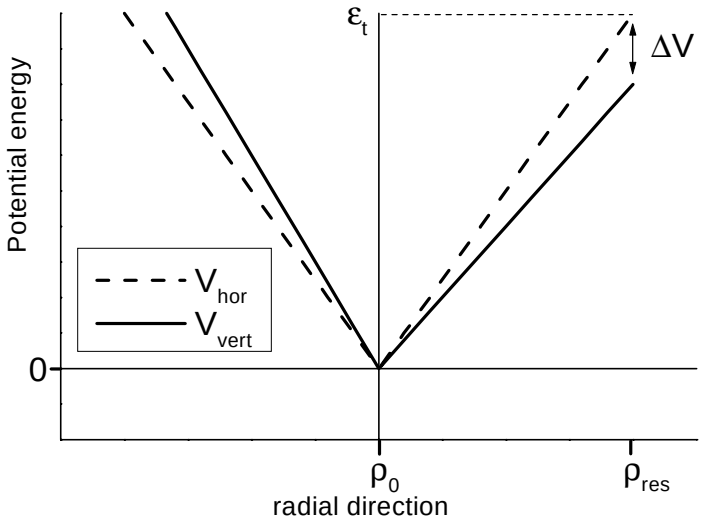

Figure 4.6: The linear trapping potential in the horizontal radial direction ($V_{\rm hor}$) and in the vertical radial direction ($V_{\rm vert}$) for the limit $kT \gg U_0$. $V_{\rm vert}$ is tilted, due to the influence of gravitation. When the difference $\Delta V \gg kT$ evaporative cooling will be one dimensional.

Harmonic limit

In the low temperature limit the radial trapping potential becomes effectively harmonic, $V_B \approx \frac{\alpha^2}{2U_0}\rho^2$, as shown in figure 4.7. Under influence of gravitational force, the position ρ_0 of the potential minimum is shifted in the vertical direction. The shift $\Delta\rho_0$ is easily calculated from $\frac{dV_{\rm ver}}{d\rho} = 0$ and yields

$$\Delta\rho_0 = \frac{m_{\rm rb} g U_0}{\alpha^2} = 1.1\ \mu\text{m}. \tag{4.83}$$

The corresponding shift in zero-point energy $\Delta\varepsilon_0$ is very small:

$$\Delta\varepsilon_0 = \frac{(m_{\rm rb} g)^2 U_0}{2\alpha^2} = 0.05\ \mu\text{K}. \tag{4.84}$$

The position of resonance $\rho_{\rm res}$ follows from $\frac{\alpha^2}{2U_0}\rho_{\rm res}^2 = \varepsilon_t$, so that condition (4.81) may be rewritten as

$$\Delta V = m_{\rm rb} g \sqrt{\frac{2U_0}{\alpha^2}}\sqrt{\varepsilon_t} \ll kT. \tag{4.85}$$

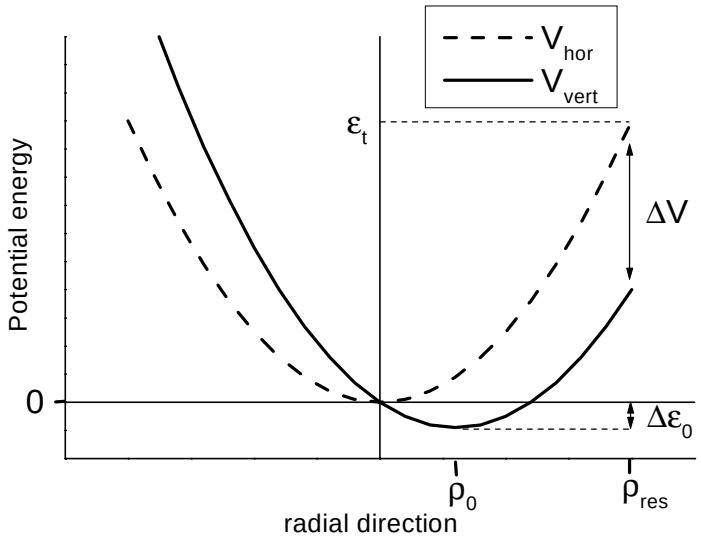

Figure 4.7: The harmonic trapping potential in the horizontal radial direction ($V_{\rm hor}$) and in the vertical radial direction ($V_{\rm vert}$) in the limit $kT \ll U_0$. $V_{\rm vert}$ is shifted, due to the influence of gravitation. When the difference $\Delta V \gg kT$ evaporative cooling will be one dimensional.

Squaring both sides of condition (4.85) and dividing by kT, one finds a condition for the temperature

$$kT \gg \eta \frac{2U_0}{\alpha^2}(m_{\rm rb}g)^2. \tag{4.86}$$

For a typical value of $\eta \sim 8$ one dimensional cooling sets in for $T < 1.8$ μK.

From conditions (4.82) and (4.86) it is clear that the effect of gravitation on the dimensionality of cooling process depends strongly on the steepness of the trapping potential: The tighter the confinement, the smaller is the influence of gravity. Given the trapping parameters as discussed in section 2, we expect the evaporation process to be 3D until close to the on-set of BEC.

However, as discussed in the preceding section, to obtain a Bose condensed sample with many atoms, adiabatic expansion is necessary to increase the life-time of the sample. In that case, inevitably cooling will become 1D, which will cause the evaporation rate to decrease over more than one order of magnitude as pointed out by [12]. From figure 4.2 one finds that for densities in the order $9 * 10^{13}\mathrm{cm}^{-3}$ losses are dominated by dipolar relaxation, corresponding to a very small collision ratio $\lambda_2 \sim 10^{-4}$. Taking into account the decrease of the evaporation rate by a factor 4η, an effective collision ratio can be expressed as

$\lambda_2^{\text{eff}} \simeq \lambda_2 * 4\eta \simeq 3 * 10^{-3}$, which still allows rather efficient evaporative cooling ($\chi \sim 3$). Thus we expect that even under conditions of 1D evaporation BEC can be reached.

Chapter 5

Conclusion

In this thesis a study of rf-induced evaporative cooling was presented, which was done explicitly for ^{87}Rb atoms in a Ioffe trapping potential. In order to determine the rf-amplitude needed for efficient evaporative cooling, the transition probability to untrapped m_F states for our five level system ($F = 2$) was calculated for realistic experimental conditions. The amplitude of the rf-field needed to maintain a constant efficiency close to unity was expressed as a function of temperature. At the start of the cooling process, at a temperature of 300 μK, we found: $B_{\mathrm{rf}} = 130 * 10^{-7}$ T. As the temperature decreases the amplitude of the rf-field may decrease due to the drop in thermal speed and or temperatures below 10 μK the amplitude may decrease even faster, due to the flattening of the trapping potential. At the final stage of the cooling process, for a temperature of 1 μK, this results in a rf-amplitude $B_{\mathrm{rf}} = 22 * 10^{-7}$ T. Apart from a lower bound to the rf-amplitude an upper bound was considered, originating from the condition that the atoms in the field center should not be affected by the rf-field. We found that for temperatures below ~ 1 μK it may not be possible to efficiently remove high energetic atoms from the trap, without inducing transitions to untrapped states in the center of the trap. Finally, the design of the rf-circuit was considered. For a two turn coil in combination with a 17 Watt amplifier the required field amplitudes can be obtained. A controllable attenuator will provide the necessary amplitude decrease.

The main part of this thesis is devoted to a detailed study of the dynamics of evaporative cooling, on the basis of the analytical model of Walraven [14]. The evaporation process was numerically simulated and we determined optimized trajectories $\varepsilon_t(t)$, reaching the on-set of BEC with minimal particle loss. The simulation predicts that the BEC transition point can be reached with less than two orders of magnitude particle loss, typically with $\sim 10^7$ atoms remaining. However, the lifetime of the sample at the BEC on-set will be short due to rapid loss from three-body recombination. Therefore, adiabatic expansion of the trapping potential in the final stage of the evaporation ramp will be necessary to increase the lifetime of the sample.

Bibliography

[1] A.Einstein, Sitzber. Kg. Preuss. Akad. Wiss (1924), p. 261; (1925), p. 3

[2] M.H.Anderson, J.R.Ensher, M.R.Matthews, C.E.Wieman and E.A.Cornell, Science 269, 198 (1995).

[3] K.B.Davis, M.O.Mewes, M.R.Andrews, N.J.van Druten, D.S.Durfee, D.M.Kurn and W.Ketterle, Phys. Rev. Lett. **75**, 3969 (1995).

[4] C.C.Bradly, C.A.Sackett, J.J.Tollet and R.G.Hulet, Phys. Rev. Lett. **75**, 1687 (1995).

[5] U. Ernst, A. Marte, F. Schreck, J. Schuster, G. Rempe, Europhysics Letters 41, 1 (1998).

[6] W.H.Wing, Prog. Quant. Electr. **8**,181 (1985).

[7] O.J.Luiten, PhD thesis, University of Amsterdam (1993), unpublished.

[8] D.Suter, *The Physics of Laser-Atom Interactions* (Cambridge University Press, 1997).

[9] J.R.Rubbmark, M.M.Kash, M.G.Littman and D.Kleppner, Phys. Rev. A **23**, 3107 (1981).

[10] A.B.Migdal and V.Krainov, *Approximation methods in Quantum Mechanics* (W.A.Benjamin, New York, 1969).

[11] H.M.J.M.Boesten, C.C.Tsai, J.Gardner, D.J.Heinzen and B.J.Verhaar, Phys. Rev. A **55**, 636 (1997).

[12] E.L.Surkov, J.T.M.Walraven and G.V.Shlyapnikov, Phys. Rev. A **53**, 3403 (1996).

[13] O.J.Luiten, M.W. Reynolds and J.T.M.Walraven, Phys. Rev. A **53**, 381 (1996).

[14] J.T.M.Walraven in *Proceedings of the SUSSP 44 conference on Quantum Dynamics of Simple Systems*, edited by G. L. Oppo, S.M. Barnett, E.Riis and M.Wilkinson (IOP, Bristol,1996).

[15] H.Wu and C.J.Foot,J. Phys. B **29**,L321 (1996).

[16] *Handbook of mathematical functions*, edited by M.Ambramowitz and I.A.Stegun (Dever, New York, 1972).

[17] W.Ketterle and N.J.van Druten, in *Advances in Atomic, Molecular and Optical Physics*, edited by B.Bederson and H.Walther (Academic Press, San Diego, 1996), No 36.

[18] J.Söding, D.Guéry-Odelin, P.Desboilles, F.Chevy, H.Inamori and J.Dalibard, cond-mat/9811339, (1998).

[19] H.M.J.M.Boesten, A.J.Moerdijk and B.J.Verhaar, Phys. Rev. A **54**, R29 (1996).

[20] A.J.Moerdijk, H.M.J.M.Boesten and B.J.Verhaar, Phys. Rev. A **53**, 916 (1996).

[21] E.A.Burt, R.W.Ghrist, C.J.Myatt, M.J.Holland, E.A.Cornell and C.E.Wieman, Phys. Rev. A **79**, 337 (1997).

[22] N.R.Newbury, C.J.Myatt and C.E.Wieman, Phys. Rev. A **51**, R2680 (1995).

[23] C.A.Sackett, C.C.Bradley and R.G.Hulet, Phys. Rev. A **55**, 3797 (1996).

[24] P.W.H.Pinkse, A.Mosk, M.Weidemüller, M.W.Reynolds and J.T.M.Walraven, Phys. Rev. A **57**, 4747 (1998).